Elastic plastic fracture behavior and effect of band-overload on fatigue crack growth rate of an HSLA steel

by

OM PRAKASH

National Institute of Technology Rourkela, Odisha (INDIA) -769008

A thesis submitted for the degree of Master of Technology in Mechanical Engineering
(Specialization: Steel Technology)
May-2014

Elastic plastic fracture behavior and effect of band-overload on fatigue crack growth rate of an HSLA Steel

A thesis submitted in partial fulfillment of the requirements for award of the degree of

Master of Technology

in

Mechanical Engineering

(Steel Technology)

By

OM PRAKASH

(Roll No. 212MM2336)

Under the supervision of

Prof. B.B.Verma
Department of Metallurgical and Materials Engineering
National Institute of Technology
Rourkela-769008

Prof. P.K. Ray
Department of Mechanical Engineering
National Institute of Technology
Rourkela - 769008

Department of Metallurgical and Materials Engineering
National Institute of Technology Rourkela- 769008
Odisha (INDIA)

Dedicated

To

My Respected Maa-Babu ji

National Institute of Technology, Rourkela

Odisha (INDIA) -769008

CERTIFICATE

This is to certify that the thesis entitled, **"Elastic plastic fracture behavior and effect of band-overload on fatigue crack growth rate of an HSLA steel"** submitted by **Mr. Om Prakash** in partial fulfillment of the requirements for the award of Master of Technology Degree in **Mechanical Engineering** (specialization of **Steel Technology)** at National Institute of Technology, Rourkela, Odisha (INDIA) is an authentic work carried out by him under our supervision and guidance. To the best of our knowledge, the matter embodied in the thesis has not been submitted to any other University/ Institute for the award of any degree or diploma.

Prof. B.B.Verma

Department of Metallurgical and Materials Engineering

National Institute of Technology

Rourkela-769008

Prof. P.K. Ray

Department of Mechanical Engineering

National Institute of Technology

Rourkela - 769008

Date:

Place:

Acknowledgement

When you start any work it will be surely finish, for successful completion of any work, it requires hard work and determination in a right direction. Behind successful completion of my work there are many people who made it possible and whose constant guidance and encouragement crowned all the efforts with success. Therefore, I would like to take this opportunity to express my sincere and heartfelt gratitude to all those who made this report possible.

First of all, I am highly grateful to my supervisor, **Prof. B.B.Verma,** Department of Metallurgical and materials Engineering, N.I.T Rourkela for believing in me and encouraging me in every step, and their great support and inspiring guidance throughout the project work, thanks for helping me to make my one of dreams comes true.

I also wish to express my deep sense of gratitude and indebtedness to **Prof. P.K.Ray**, Department of Mechanical Engineering, N.I.T Rourkela, for their inspiring guidance and valuable suggestion throughout this project work.

I would like to express my grateful thank**s** to **Dr. S. Sivaprasad,** Principle Scientist, National Metallurgical Laboratory Jamshedpur, for their kind support, and give us time for valuable suggestion regarding project work.

I would gratefully acknowledge to Rourkela steel plant (RSP- SAIL), for providing HSLA steel for this study, and I also great thankful to Mr. C. Muthuswamy, Dy. General Manager (R&C Lab.) RSP- SAIL for providing chemical analysis of material, and his positive feedback.

My sincere thanks to our entire Lab mate friends who have great support in every level of difficulties and make them easy. It is my pleasure to acknowledge **Mr. Vaneshwar kumar Sahu** for their great kindness and continuous support in my all doubts and problem. I also thank to Mr. Shyamu Hembram (Lab Assistant, MM), Mr. D. Sudhakar and Mr. Suhan Bekal (BiSS Technical assistant) for their constant support during my work and operational support.

Special thanks to my god (**Maa-Babu** ji) and family members, without their blessings and support, I could not have reached this destination.

Last but not the least, I wish to place my deep sense of thanks to all my friends especially to Mr. Navratan Kumar and Mr. Ajit Kumar for their cooperation and critical suggestion during my project works and studies.

Om Prakash
(May 2014)

Abstract

Study of fracture toughness and fatigue crack growth behavior are important parameters of structural materials. These parameters can be used to predict their life, service reliability and operational safety in different conditions. The material used in this investigation is an HSLA steel.

In the first part of this investigation elastic plastic fracture toughness (J_{Ic} and δ_{Ic}) were measured, by resistance curve method. Tests were carried out on CT specimens, using unloading compliance technique. These tests were conducted at three different displacement rates. It is observed that fracture toughness decrease with increasing rate of displacement.

In the next part of this investigation effect of single overload and band-overload on fatigue crack growth of same steel were studied. These tests were conducted on CT specimens. Single overload and band overloads were applied under mode-I condition, during constant amplitude (tension-tension) fatigue crack growth test. It is observed that overload and band-overload applications resulted retardation on the fatigue crack growth rate in most of the cases. It is also noticed that maximum retardation took place on application of seven successive overload cycles.

Keywords: Fatigue crack growth rate, Stress intensity factor, Fracture toughness, Overload, Band-overload, CT specimen, J_{Ic} and δ_{Ic}, Resistance curve.

CONTENTS

List of figures

List of tables

Nomenclature

B	specimen thickness (mm)
Be	effective thickness for side-grooved specimens (mm)
B_N	net specimen Thickness (mm)
W	specimen width (mm)
a_o	original crack size *(*crack length measured from center line of pin hole of the specimen) (mm)
a_n	notch length (mm)
a_f	final crack length (mm)
$(a/W)_{ol}$	ratio of crack length to width of specimen at overload point
f	cycle frequency (Hz)
f_{ol}	overload cycle frequency (Hz)
a_i	crack length corresponding to the 'i$^{\text{th}}$' (initial) step (mm)
a_{ol}	crack length at overload (mm)
Δa	crack extension (mm)
b_{o}	original (un-cracked) ligament length (mm)
b	remaining ligament length (mm)
K_{max}	maximum stress intensity factor in a cycle $\left(MPa\sqrt{m}\right)$
K_{min}	minimum stress intensity factor in a cycle $\left(MPa\sqrt{m}\right)$
ΔK	stress intensity factor range $\left(MPa\sqrt{m}\right)$
K_{th}	threshold stress intensity factor $\left(MPa\sqrt{m}\right)$
R	loading ratio or stress ratio
R_{ol}	overload ratio
σ_{max}	maximum stress in a cycle (MPa)
σ_{min}	minimum stress in a cycle (MPa)
σ_{YS}	yield stress (MPa)
σ_{Y}	effective yield strength (MPa)
$\Delta\sigma$	stress range (MPa)
E	Young's modulus of elasticity (MPa)
$\text{d}a/\text{d}N$	crack growth rate (mm/cycle)
P_{max}	maximum load of constant amplitude load cycle (N)
P_{max}^{ol}	maximum load at overload (N)
δ	crack-tip opening displacement (CTOD) (mm)
N	number of cycles or fatigue life (cycle)

Chapter-1

INTRODUCTION

1. INTRODUCTION

1.1. Background

Fatigue and fracture are common cause of service failure of engineering components and structures.

To study about fatigue and fracture related problem is very important of any kind of machine parts, components and engineering structure that is related to various type of loading condition during their operation, so realistic fatigue crack growth and fatigue life prediction is one of the most importance part in terms of economic and safety point of view.

Fracture mechanics is based on the inherent assumption that there already exists a crack in a work-component or engineering structure. The crack may be man-made as a key- hole, a grooves, a notch, a re-entrant corner, or a slot, etc. The crack may exist within a component due to manufacturing defects like slag or impurities inclusion, cracks in a weld-ment or heat affected zones due to irregular cooling and existence of foreign particles. A serious crack may be nucleated and start growth during their service of the machine elements or structure (fatigue caused cracks, nucleation of cracks in notches due to environmental dissolution).Fracture mechanics is also applied to crack growth under fatigue loading condition. Initially, the fluctuating load nucleates a crack, which then propagates slowly and finally the crack growth rate per cycle accelerated and followed the fast fracture. Subsequently comes to the stage when the crack-length is long enough to be considered critical for a catastrophic fracture failure.

Fracture mechanics is now applied comprehensively to important fields like thermal, nuclear engineering, aerospace industries, space ships, rockets, piping, offshore structures, etc. Critical components of thermal, nuclear power plants are made from very tough materials; but they have too failed catastrophically once in a while. In addition, fracture mechanics can be used to evaluate the suitability-for-service, or life extension, of existing structures.

The fatigue crack growth rate may be significantly affected by the application of overload cycles [1]. In fatigue crack growth, load applied in the form of a single or band overloads may follow either in mode I or mixed-mode (mode I and II). Mixed-mode overloads are common in case of,

turbine blade and shafts, aircraft structures, railroads in pressure vessels, weld-ments etc. [2]. It has been evidenced that a pure mode-I overload and multiple overloads leads to maximum crack growth retardation, however in mode-II overload has least effect on fatigue crack growth retardation [2, 3].

Most of engineering machine parts and structures are failed by fatigue and fracture causes problem [4]. Our aim to understand how materials fail and how crack start and propagate, how we control it and our ability to prevent such failures.

Fatigue resistance of engineering structures and components is mostly affected by the existence of stress raisers such as key way, fastener holes, joints, notches, environmental conditions and corrosion pits which promote as crack nucleation sites for fatigue cracking, during operation, start cracks nucleate from these sites and continually propagate till final failure takes place when the fatigue crack length approach a critical dimension [5]. From economical and safety point of view a costly structure and machine component cannot be replaced from service simply on detecting a fatigue crack during operation. Therefore, reliable valuation of fatigue crack growth and fatigue life prediction are crucial so that the parts/structures can be well-timed serviced or replaced.

Fracture toughness is a key parameter for evaluating critical strength of engineering structural in the given environmental condition. CTOD and the *J*-Integral are two important fracture evaluation parameters in EPFM and its applications are already well developed all over and used in industrial and structural applications [6].

The fracture toughness test can be conducted for different-different conditions based on the toughness parameters, K_{Ic}, J_{Ic} or CTOD. The value measured from the J-integral test is J_{IC} (critical value of J at crack initiation) which give a single point measured value of elastic plastic fracture toughness [6]. A fracture toughness test measures the resistance of a material against crack extension. These tests may produce either a unique single value of toughness or a resistance curve, where a fracture toughness parameter such as *K*, *J*, or δ is plotted against the crack extension. A particularly single fracture toughness value is usually adequate to explain a test that fails by cleavage, because this fracture mechanism is typically unstable [4]

1.2 Plan of work

The overall work plan are divided in two parts as initial parts of work on basic material characterisation as preliminary work and main work in which main objective and investigations are focused. Here all the work plan can be visualized from flow chart as shown in figure 1.1.

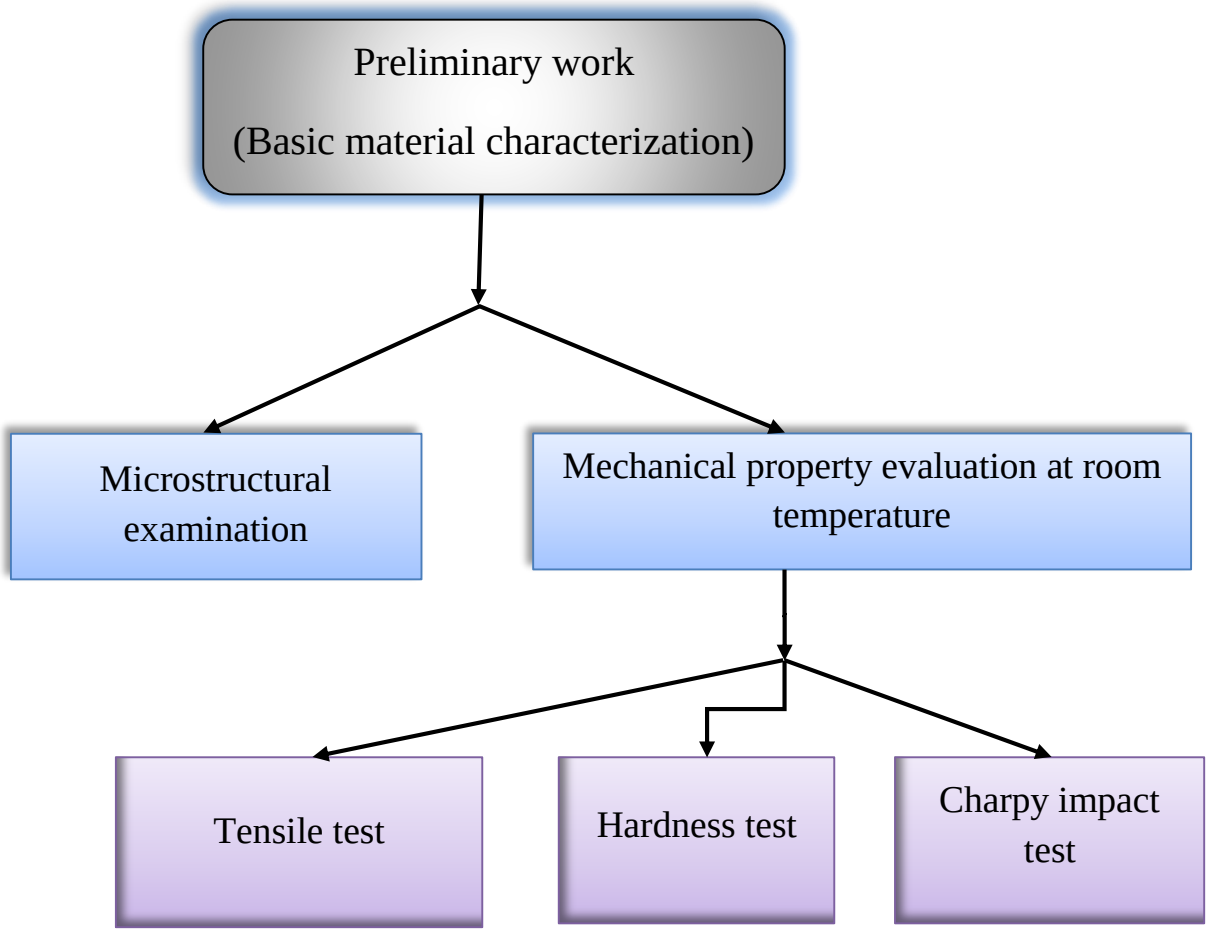

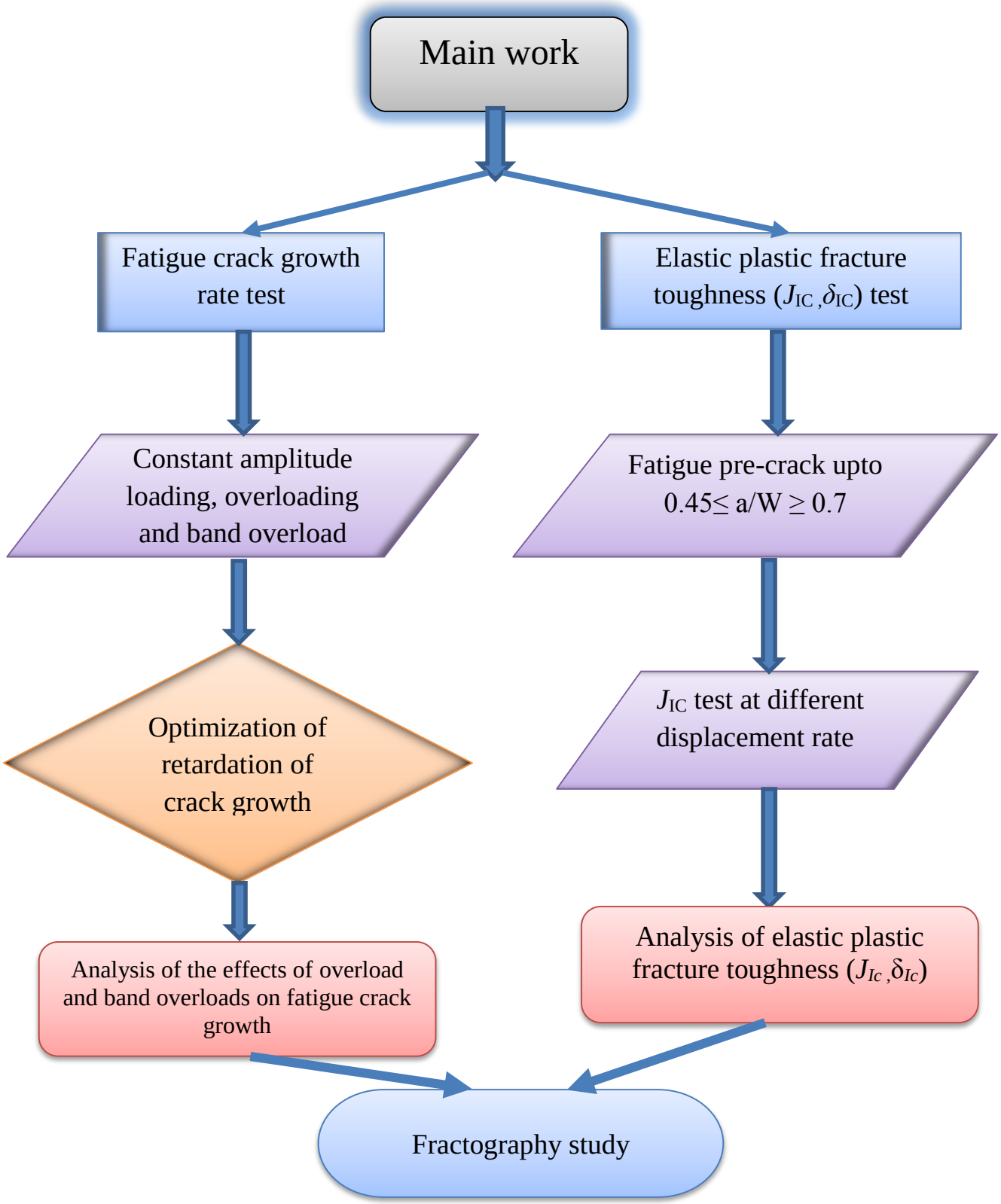

Figure 1.1 Flow chart of work plan

1.3 Objective

The aim of present investigation are-

- To study the microstructural examination and evaluate basic mechanical properties of supplied HSLA steel at room temperature.
- To study the elastic plastic fracture toughness (J_{Ic} and δ_{Ic}) of material at different displacement rate and predicting its effects on fracture toughness of the material.
- To study the effect of overload and band overloads applications on fatigue crack growth and fatigue life.
- To study the mechanism of fatigue crack growth under band overloading and elastic plastic fracture toughness through fractogrpahy.

1.4 Structure of thesis

Present investigation is divided in to six chapters whose overall structure has been divided in to two parts as preliminary work and main work and is diagrammatically represented by flow chart in figure 1.1. The first two chapters 1 and 2 deals with an introduction and a brief review of literature**.** Chapter 3 and 4 describes the details of materials and experimental procedure and their results with discussion respectively. Chapter 5 deals with the concluding remarks and possible future work. The list of references is presented at chapter 6 of the thesis.

Chapter 2

LITERATURE REVIEW

2.1 Introduction

In fracture mechanics mainly studied about how any structure or components get failed in different type loading and environment condition, in present work fracture toughness mainly concentrate about elastic plastic fracture toughness (J_{Ic} and δ_{Ic}) and effect of band overload on fatigue crack growth and fatigue life

2.2 Fracture mechanics

Fracture mechanics is the field of applied mechanics which deal about how to cracks propagation in materials and when its goes to be critical, and its approaches to solid mechanics to analyze the main driving force on a crack initiation and those of investigational solid mechanics to describe the materials resistance to fracture or failure.

Notches, slots, key way hole and other structural discontinuities are often common in solid materials, and this lead to assist the initiation of cracks. A sharp cracks and its further growth are once in a while complex to investigate and predict, because the actual driving stresses and strains at a crack tip are completely not known with the necessary accuracy. In fact, this is the reason the classical failure theories, sophisticatedly simple as they are not satisfactorily useful in dealing with notched and geometric discontinuities members. A powerful modern methodology in this area is fracture mechanics, which was originated by A. A. Griffith in 1920 and has grown in depth and scope extremely in recent decades. The aim of fracture mechanics to raise the engineers, researches and scientist awareness to a quantifiable, practically more valuable approaches in dealing with the stress concentrations and stress raiser driving parameters as they affect service life, and operational durability.

2.3 Classification of fracture mechanics

Fracture mechanics can be broadly classified in two ways:

1. Linear elastic fracture mechanics (LEFM)
2. Elastic plastic fracture mechanics (EPFM)

2.3.1 Linear elastic fracture mechanics (LEFM)

LEFM is the oldest basic theory of fracture that deals with the sharp cracks in linearly elastic bodies. The concepts of LEFM are only applicable to the materials that obey Hook's law [4]. In LEFM studies were first assumes that the material is isotropic and linearly elastic, by this assumption, the stress-strain field near the crack tip is analyzed using the concepts of theory of elasticity. When the driving stresses in front of the crack tip exceed the materials fracture toughness, the crack will start to grow.

Again, LEFM is applicable only when the in-elastic deformation is very small as compared to the size of the crack that is called small-scale yielding. If large regions of plastic deformations established before the crack grows, EPFM must be used.

Most of formulas and mathematical relationship were derived for either plane strains or plane stresses conditions, accompanying with the three basic modes of loadings on a crack subjected body that is as-

Mode I - opening or tensile mode (the crack faces are pulled apart) and the displacement is normal to the crack surface.

Mode II - sliding or in- plane shear (the crack surfaces slide over each other) and the displacement is in the plane of the plate the separation is anti-symmetric and the relative displacement is normal to the crack front.

Mode III - tearing or out of plane shear.

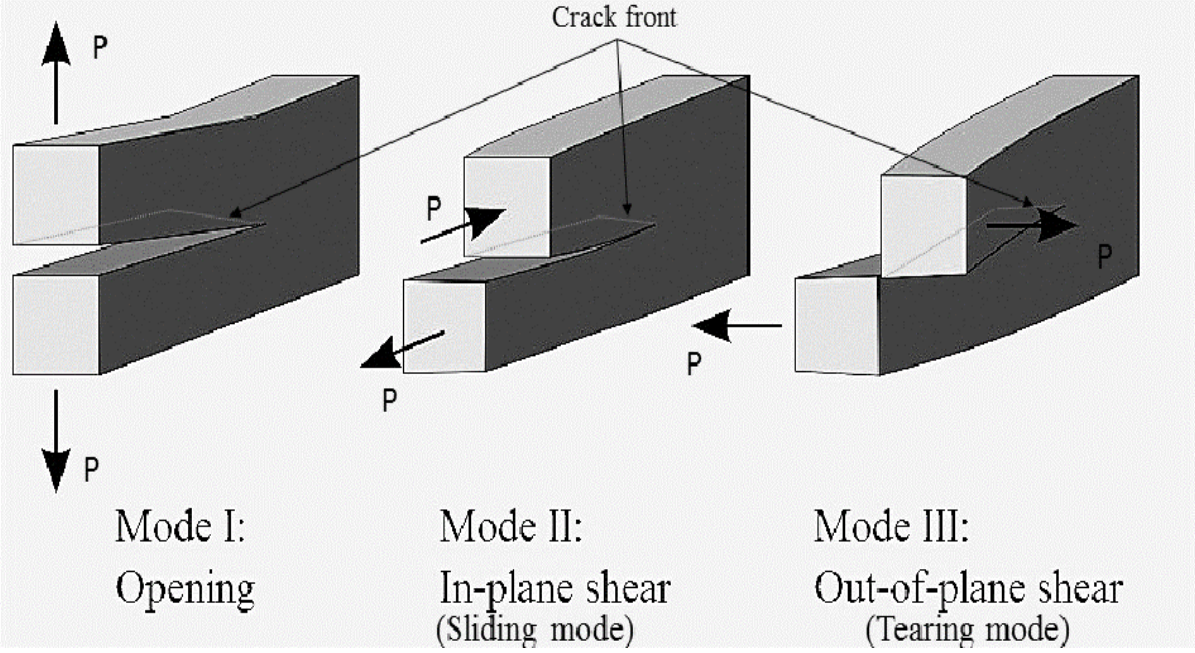

Figure 2.1 Modes of deformation or fracture.

2.3.2 Elastic plastic fracture mechanics (EPFM)

EPFM is the theory of ductile fracture, generally characterized by stable crack growth (plastic deformation) the fracture process is accompanied by developing of large plastic zone at the crack tip [4]. By idealizing elastic-plastic deformation as non-linear elastic, J.R. Rice proposed *J*-integral, for regions beyond LEFM. In loading path elastic-plastic can be modeled as a non-linear elastic but not in unloading part [7].

EPFM is recommended to analyse the relatively large plastic zones near crack tip of cracked body. EPFM assumption that material is isotropic and following elastic-plastic nature. Based on this assumption, the strain energy fields or opening displacement near the crack tips are analysed. When the applied energy or opening displacement exceed the critical value, the crack will start to grow. The term elastic-plastic is generally used in this approach, because of nonlinear-elastic behaviour of the material. Here difference between them are clearly shown by below figure 2.2.

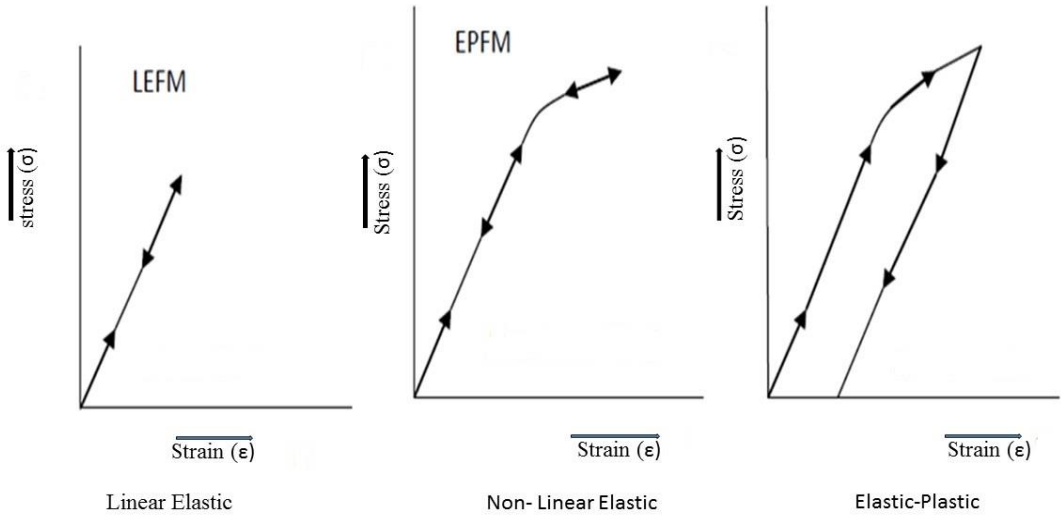

Figure 2.2 Difference between LEFM, EPFM shown by stress strain diagram

In case of EPFM generally use the *J*-Integral (J_{Ic}) or CTOD (δ). Crack tip opening displacement (CTOD) suggested by Wells, popular in Europe, and the *J*-Integral proposed by J.R. Rice [7], widely used in the United States However, most of investigator found that a distinctive correlation between *J* and CTOD exists for a material. Thus, these two parameters are valid in describing crack tip toughness for nonlinear and elastic plastic materials.

2.4 Fracture toughness

Fracture toughness is a property which defines as the ability to resist fracture, and measures in terms of resistance to crack extension; it is one of the most essential properties of any material for most of design and working applications. If a material has showing much more fracture toughness it will mostly go through a ductile fracture. Brittle fracture is also very significant property of materials with less fracture toughness [8].

Fracture mechanics, which mostly leads to the concept of fracture toughness, was broadly based on the work of Griffith A. A. who, among other things, studied the manners of cracks in brittle materials [9].

The experimental measurement and mathematical based conceptual analysis of fracture toughness playing a very important role in application of fracture mechanics methods to structural integrity valuation, damage tolerance design, fitness-for-service evaluation, and residual strength analysis for different structures and engineering components as automotive, ship, pressure vessels, and aircraft structures.

The stress intensity factor *K* (or its equivalent parameters – the elastic energy release rate *G*), the *J*-integral, CTOD (δ), and the crack-tip opening angle (CTOA) are the key parameters mostly used in fracture mechanics. The *K* factor was introduced in 1957 by Irwin [10] to deal about the intensity of elastic crack-tip fields, and represents the LEFM. The *J*-integral was proposed in 1968 by J. Rice [7] to describe the intensity of elastic plastic crack-tip fields, and represents the EPFM. The CTOD concept was introduced in 1963 by Wells [11] to assist as an engineering fracture parameter, and can be equivalently used as *K* or *J* in practical applications. By most of research and experimental results shows that the crack depth, specimen physical parameters, crack configuration and geometry, loading condition all are have a mostly effect on the fracture toughness analysis and investigation *(K, G, J* and CTOD). These effects are mentioned as constraint effect on fracture toughness. [12]

2.5 Fracture toughness testing

2.5.1 Plane strain fracture toughness (K_{Ic}).

The linear elastic fracture toughness of a material is evaluate from the crack driving stress intensity factor (*K*) at which a small thin crack in the material initiates to grow. It is represented by K_{Ic} (critical stress intensity factor value at mode-I loading condition). The limiting value of stress intensity factor required to initiate crack extension in plane strain condition at the zone near the tip of a thin crack is called plain strain fracture toughness.

2.5.2 Elastic plastic fracture toughness *(J_{Ic}* and CTOD*)*

The *J*-counter integral has greatly employed for non-linear materials for their fracture characterisation. By idealizing elastic-plastic deformation as non-linear elastic materials, J.R. Rice [7] delivered the basis for covering important parameters of fracture mechanics approach well beyond the validity limits of LEFM. The limiting value of the *J*-integral (which is a line or surface integral used to describe the fracture toughness of a material having significant elastic-plastic behavior before fracture) required to initiate crack extension from a pre-existing crack. A large significant plastic zone at near the crack tip makes a material tough.
The plane strain fracture toughness (J_{Ic}) is define as the resistance to crack-extension under conditions of plane strain in mode-I for very slow rates of loading- unloading or significant plastic deformation. J_{Ic} is used for the evaluation of crack-extension resistance near the initiation of stable crack extension. A typical *J–R* curve is a graphical plot of resistance to crack extension, (physical crack extension) for ductile materials. A method to determine the plane strain fracture toughness J_{Ic} near the onset of ductile crack growth was proposed initially by Clarke et al. [13]. Load line compact specimens and SENB test specimens with the ratio of crack length to width $a/W \geq 0.5$ were suggested for use in a fracture toughness test. [12]

2.5.2.1 J and CTOD (δ) test procedure

The steps are

- Selection of specimen (CT, SENB or DC (T)).
- Fatigue pre-cracking (Notch plus fatigue pre-crack must be a/W= 0.45 to 0.7).
- J_{Ic} and δ_{Ic} testing.
- Data analysis.
- Determination of provisional J_{Ic} or $\delta_{Ic.}$
- Final check for validity.

By ASTM E 1820-13 [14] has two alternative methods for *J* and CTOD (δ) tests:

1. Basic procedure and
2. Resistance curve procedure

Resistance curve method are mostly popular because it is single-specimen and unloading compliance technique for evaluation of fracture toughness of metallic materials and now a days mostly used. The *J-R* and δ-*R* curve is a plot of δ or *J* versus Δ*a* (crack extension). Basic procedure required multiple specimen and its conservative and complex analysis as compared to resistance curve method. Data analysis for J_{Ic} and δ_{Ic} are deals on chapter-3.

2.6 Affecting variables of fracture toughness

In brief the affecting variables are-

A. Metallurgical factors: microstructure, inclusions, impurities, composition, heat treatment, thermo-mechanical processing.

B. Test conditions: specimen thickness, strain rate, temperature and working environment.

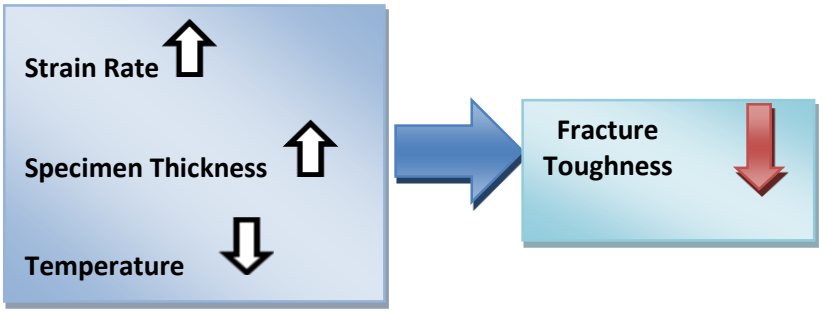

Figure 2.3 Major affecting variables of fracture toughness

2.7 Literature on the effect of displacement rate or strain rate on fracture toughness

Fracture toughness value is very significant parameters for design and control of failure of any structures before engineer can use the fracture toughness values in design for fracture control failure analysis or fitness for service, the critical fracture toughness value for particular loading rate and service condition must be studied[15].

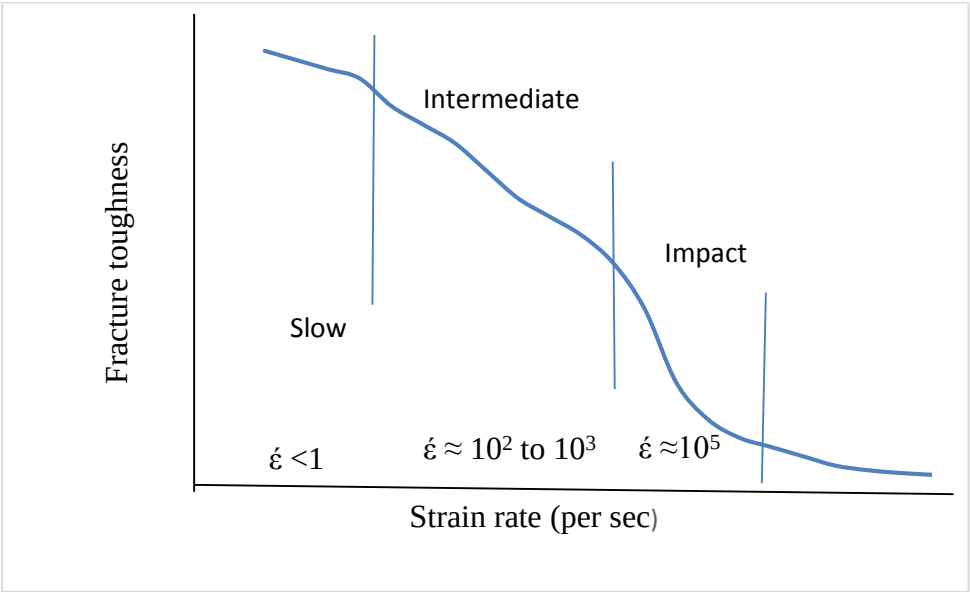

Figure 2.4 Effect of strain rate on fracture toughness

Several investigator were studied on effect of strain rate on fracture toughness and mostly they were observed that fracture-toughness decreases significantly with increasing displacement rate or loading rate or simply say strain rate. In general the fracture toughness of structural materials, particularly steels increases with increasing temperature but decreases with increasing loading rate [15].

Most of fracture toughness test were conducted at slow strain rates, because some materials are strain rate sensitive, their fracture toughness value at faster loading rates can be quite different from the measured in a slow fracture toughness test. Low strength structural steels shows a large change in fracture toughness for different loading rates [15].

However little work has been done on the effect of displacement rate in non- linear elastic plastic or fully plastic fracture mechanics or the critical *J*- Integral (J_{Ic}) and critical CTOD (δ_{Ic})

S. Kodma et al. [16] the study of the effect of strain rate on the J-Integral were had been conducted on half inch thickness CT specimen made by Boron steel (SAE 10B35), at four different cross head speed (Displacement rate) as 0.1, 1.0,10.0 and 100mm/min. By experimental results they were found that J_{Ic} values decreases with increasing displacement rate.

2.8 Charpy Impact toughness test

The Charpy impact test is a very high strain-rate dynamic test in which a test specimen U-notched or V-notched in the middle is used, and measured the amount of energy absorbed by a material before fracture. This absorbed energy is a measure of the impact toughness and use as a parameters to study temperature dependent ductile-brittle transition behaviour of materials. It is mostly use in industry to measure impact toughness and DBTT of materials because of it is very easy to prepare the specimen and easily conduct and also get the results quickly and cheaply.

2.9 Fatigue and fatigue failure- mechanism

Metal fatigue is define as a process which causes premature failure or unwanted damage of an engineering parts or component subjected to repeated reversed or cyclic loading. Most of machine parts and components subjected to repeated reversed or cyclic loading are found to fail, when the actual maximum stress are below the actual ultimate strength of the material, and sometimes at stress values even below the actual yield strength of materials [17]. Fatigue is estimated to cause 80- 85% of all operational service failures of metallic components and structures such as ships, bridges, aircraft, machine components, etc. are occurring under variable or constant fluctuating load or cyclic stresses, failure can occur at stress significantly below than the actual ultimate tensile or yield strengths of material under a static load condition.

2.9.1 Stages of fatigue crack growth

Fatigue proceeds in three different stages as:

1. Crack initiation

   Region–I:

   - Early development of damage.
   - difficulty in defining crack size (dislocation, micro-crack, porosity etc.)

2. Crack propagation

   Region–II- crack growth

   - Deepening of initial crack on shear planes.
   - crack can first be observed in an engineering sense.

   Stage II crack growth

   - well-defined crack growth on a planes normal to maximum tensile stress.
   - crack growth can be observed.

3. Final catastrophic failure

   - ultimate failure of materials.

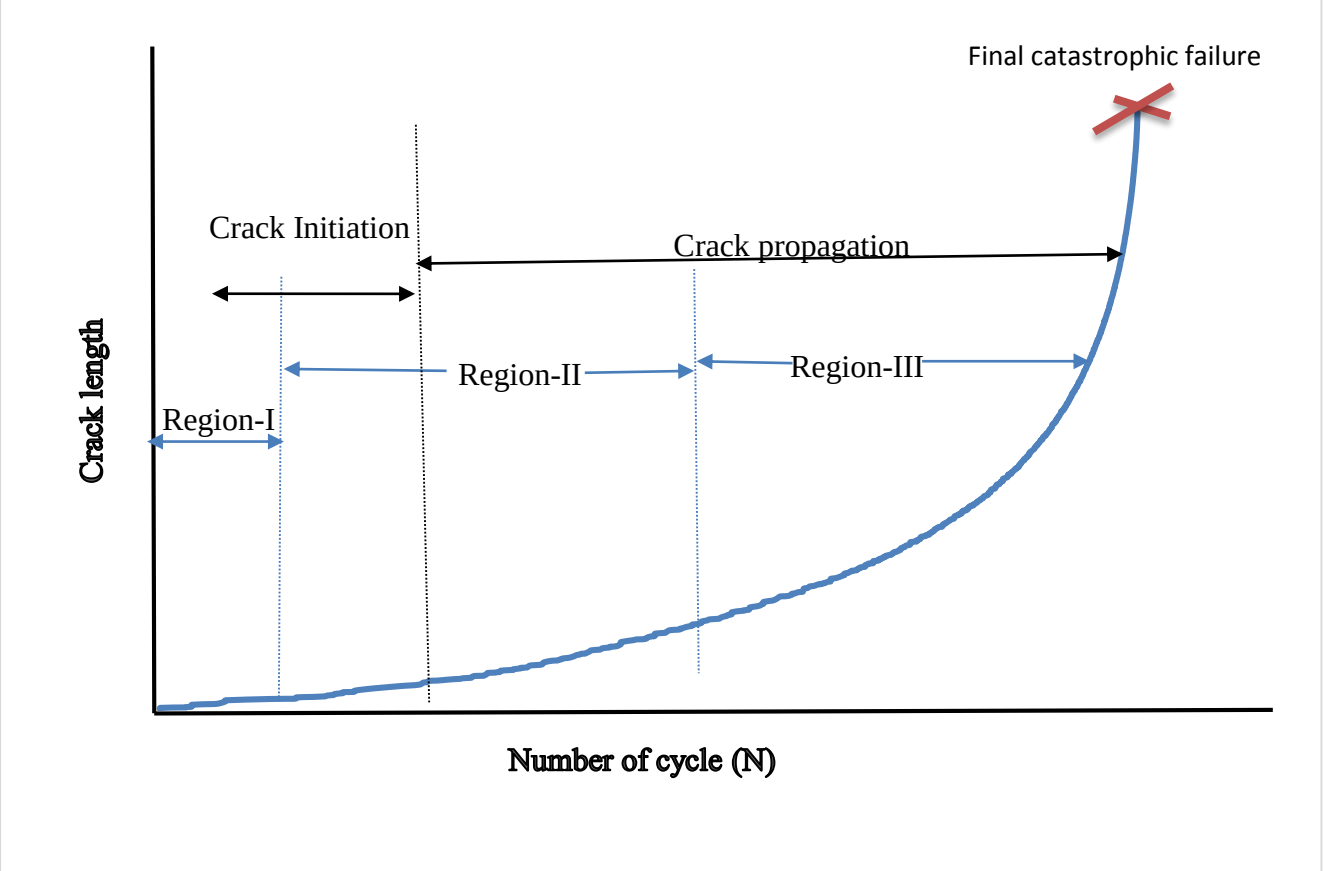

Figure 2.5 Schematic relation between crack initiation, propagation and catastrophic failure.

2.9.2 The macro mechanism of fatigue failure

The micro mechanism of fatigue failure is briefly discussed as-

1. Crack initiation - It is occur in the areas of localized stress concentration (near stress raisers) such as key ways, notches holes, slots, also cracks may start at surface, and due to geometrical discontinuity, and sites of inclusions and existing cracks.

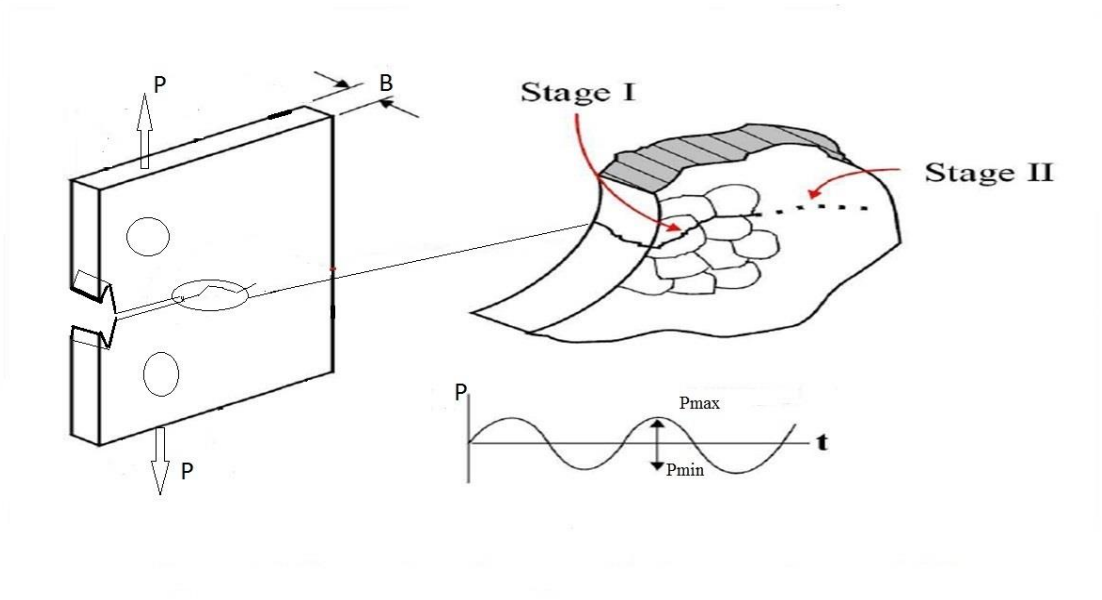

Figure 2.6 Stages of fatigue crack growth shown by compact tension specimen during fatigue crack growth test

2. Incremental crack propagation - By further increasing the stress levels and the process continues, propagating the fatigue cracks across the grains or along the grain boundaries, by this slowly increasing the crack size.

3. Final catastrophic failure - As the area becomes too deficient to resist the induced stresses results as a sudden fracture in the structures or a machine components. At the final stage of fatigue material ultimately failed.

2.10 Types of Fatigue

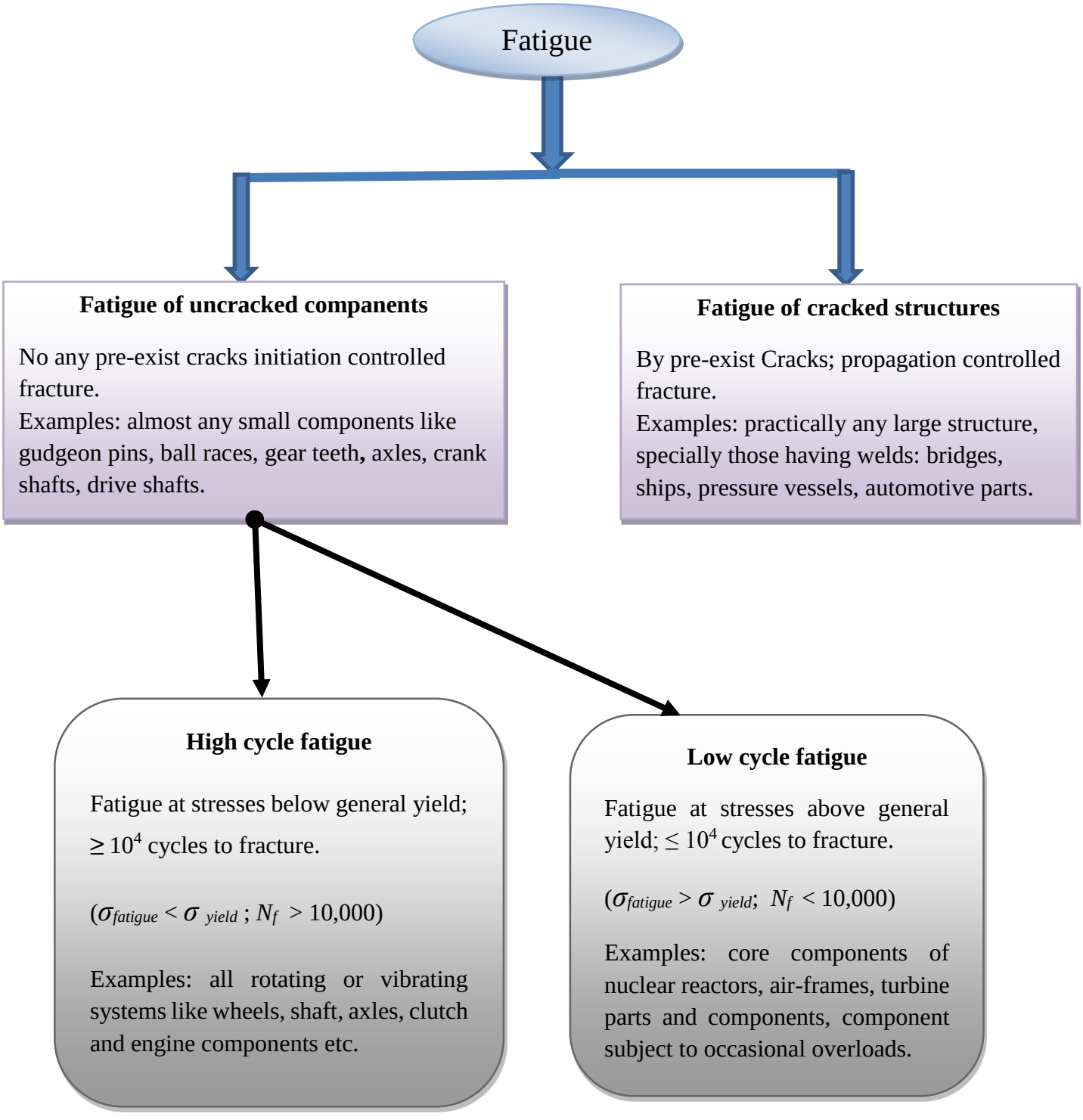

Figure 2.7 Flow chart of types of fatigue with details.

2.11 Fatigue crack growth

The common of fatigue life may be taken up in the propagation of a crack. By the application of fracture mechanics approaches it is likely to predict the number of cycles used up in growing a crack to some specific length or to final fracture. The effects of load ratio on the fatigue crack growth behavior are generally available for some standard geometric specimens [18]. Fatigue crack growth behavior mostly depends on the state of stress near at the notch tip zone, the geometry, and shape of the key hole, notches and loading parameters etc.
The aircraft industry mostly concerned about crack growth and proper and realistic prediction of fatigue crack growth for safe-life or fail-safe design approach. Thus by well knowing the material crack growth behavior and characteristics with regular examinations, a cracked structures or machine component may be kept in operational service for an extended valuable life [17].

2.12 Different regions of crack growth rate curve

Theoretical and investigational linear elastic methodologies tries to define the stable and unstable crack growth by a fatigue crack growth which can be defined as incremental crack growth (*da*) divided by increment in number of cycles (*dN*). This fatigue crack growth rate (*da/ dN*) and stress intensity factor range can be inter-related by Paris law as $da/dN = C(\Delta K)^m$ (where *m* and *C* are material constants and $\Delta K = K_{max} - K_{min}$. If a graph is plotted between log (*da/ dN*) versus log (ΔK) it will be follow the trends, that is shown in figure 2.8. This graph can be divided in to three regions. The most common way to represent fatigue crack growth rate data is a plot between log *da/dN* versus log ΔK.

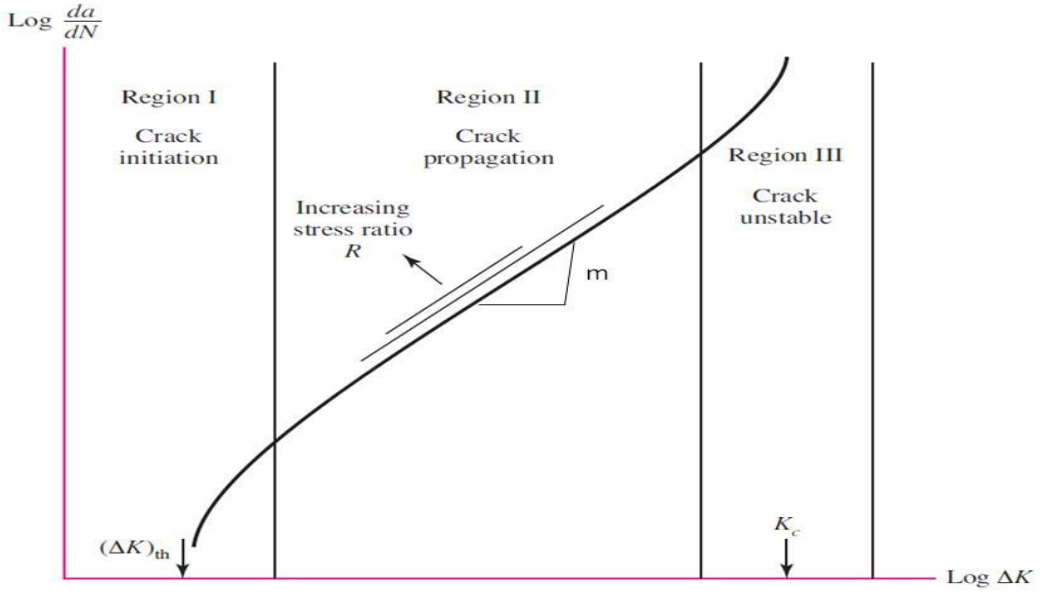

Figure 2.8 Three different regions of crack growth rate curve.

Region-I*:* This region is described as crack initiation zone in which increase in log *da/dN* asymptotically with log (*ΔK*). It is the fatigue threshold zone where the *ΔK* is value is not enough to propagate a crack. Crack cannot be initiated until and unless *ΔK* reaches certain threshold value known as ΔK_{th}. Below this the growth in *da/dN* is too low that cannot be measured experimentally. This regions is normally contributed by crack nucleation and early growth initiation state. Above threshold *da/dN* will increase in a steep manner.

Region II: It is also called as crack propagation or Paris regime in which crack growth rate is followed a linear variation with respect to increasing in log *ΔK*. This region is characterized by stable crack growth.
Region III: This zone is described by fast fatigue crack growth rates. Since the material is approaching the point of unstable fracture, and the K_{max}) of the cycle reaches to critical fracture toughness (K_C) of materials.

2.13 Literature on effects of overload and band-overload on fatigue crack growth:

An overload is a pulse or a set of pulses of higher amplitude on a constant amplitude fatigue loading as shown in figure 2.10 and 2.11 the crack propagation rate retards considerably after the overload pulse [19, 20]. During region- II of fatigue crack growth, overloads can have a very significantly effect on fatigue life. During the overload the very high crack tip strain induces a large zone of plastic deformation ahead of the crack. During unloading elastic material tries to regain its original state, however the plastic zone cannot regain the original state and, therefore, compressive residual stresses are developed in the locality of the crack tip.
By application of overload and band overload on fatigue cycle results in a plastic volumetric expansion that acts to close the crack. Any subsequent cycles have, first of all, to rise above the cracks pre-compression before causing damage. Therefore the crack growth rate is retarded. This is demonstrated in Figure 2.12, this phenomena is well-known as crack retardation. This influence retards the fatigue crack growth rate until it has not to successfully propagate through the affected zone, after that it continues in general.
Several investigators [21-28] observed that changes in magnitude of cyclic load may result in retardation or acceleration in fatigue crack growth rate. Extensive published data show that the rate of fatigue crack growth rate under constant amplitude cyclic load fluctuation can be retarded significantly as a result of application of single or multiple tensile overload cycle having peak load greater than that of the constant amplitude loading cycles. Von Euw [29] observed that the minimum value of fatigue crack growth rate did not occur immediately after the high tensile load cycle but that the rate of growth retardate to a minimum value. This retardation region has been termed as delayed retardation, shown on Figure 2.9 Several models have been proposed to explain the phenomenon of crack growth delay. In general, these models attribute the delayed behavior to crack-tip blunting, residual stresses [30, 31] crack closure [32], or a combination of

these mechanisms. A crack tip blunting model advocates that high tensile load cycles cause crack tip blunting, which in turn causes retardation in fatigue crack growth at the lower cyclic load fluctuations until the crack is re-sharpened. The residual stress model suggest that the application of a high overload cycle generate residual compressive stresses in the locality of the crack tip that reduce the rate of fatigue crack growth rate. Finally, the crack closure model postulates that the delay in fatigue crack growth is caused by the formation of a zone of residual tensile deformation left in the wake of a propagating crack that causes the crack to remain closed during a portion of the applied tensile load cycle. Consequently, fatigue crack growth delay occurs because only the portion of the overload cycles above the crack opening level is effective in extending the crack.

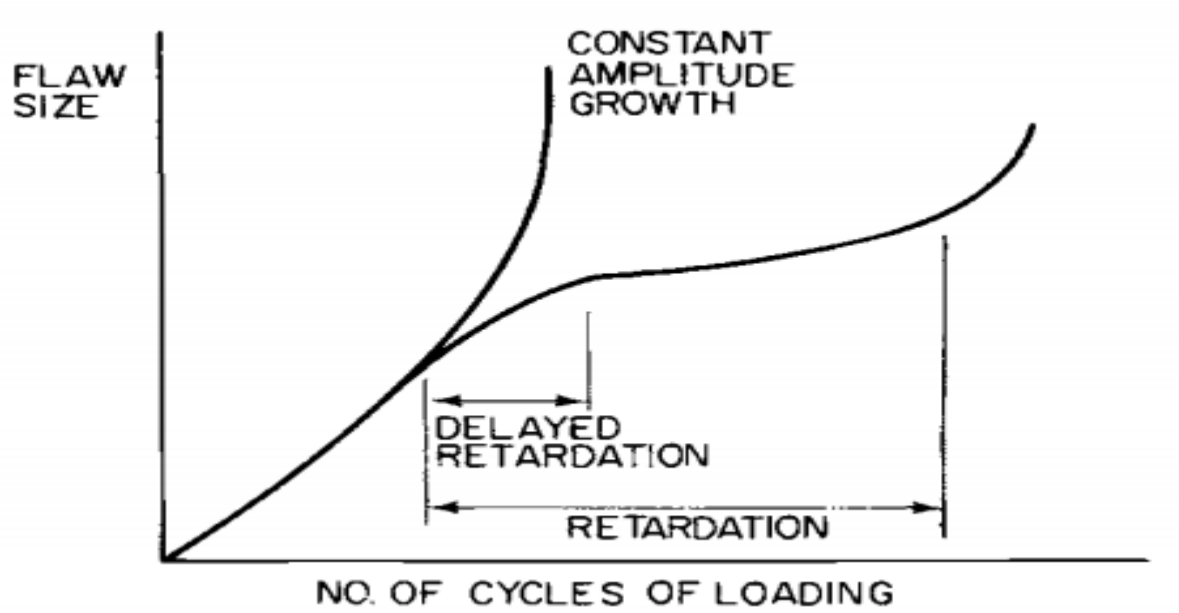

Figure 2.9 Retardation in fatigue crack growth by overload and band overload application during test.

Fatigue crack growth delay has been shown to be strongly dependent on all the loading variables, such as the stress intensity factor fluctuation, of the high tensile load cycle, the ΔK for the constant amplitude cycles (Fig. 9.20) [33], the stress ratios of these ΔK values and the number of constant amplitude cycles between the high tensile load cycles [33-36]. Extensive research is necessary to further our understanding of the significance of these variables in order to develop equations that can be used to predict accurately the fatigue life of components subjected to single or multiple high tensile load cycles.

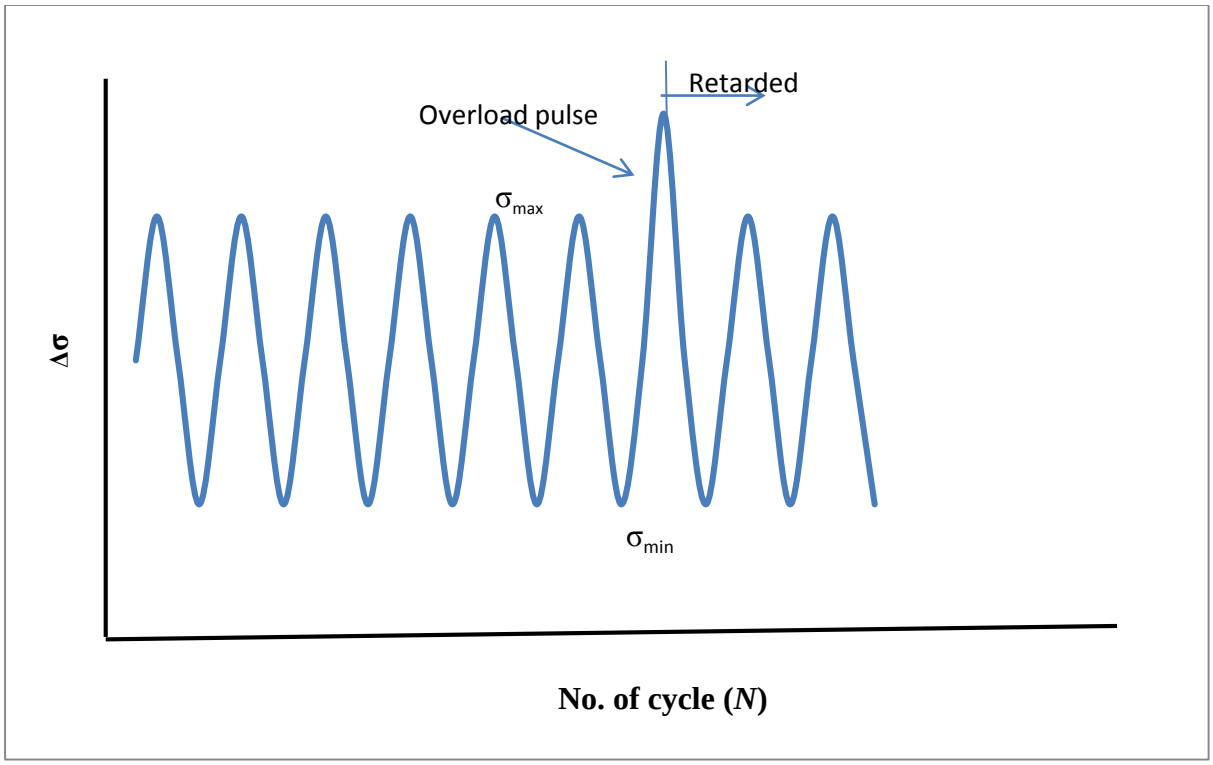

Figure 2.10 Single overload pulses on the constant amplitude fatigue load cycle.

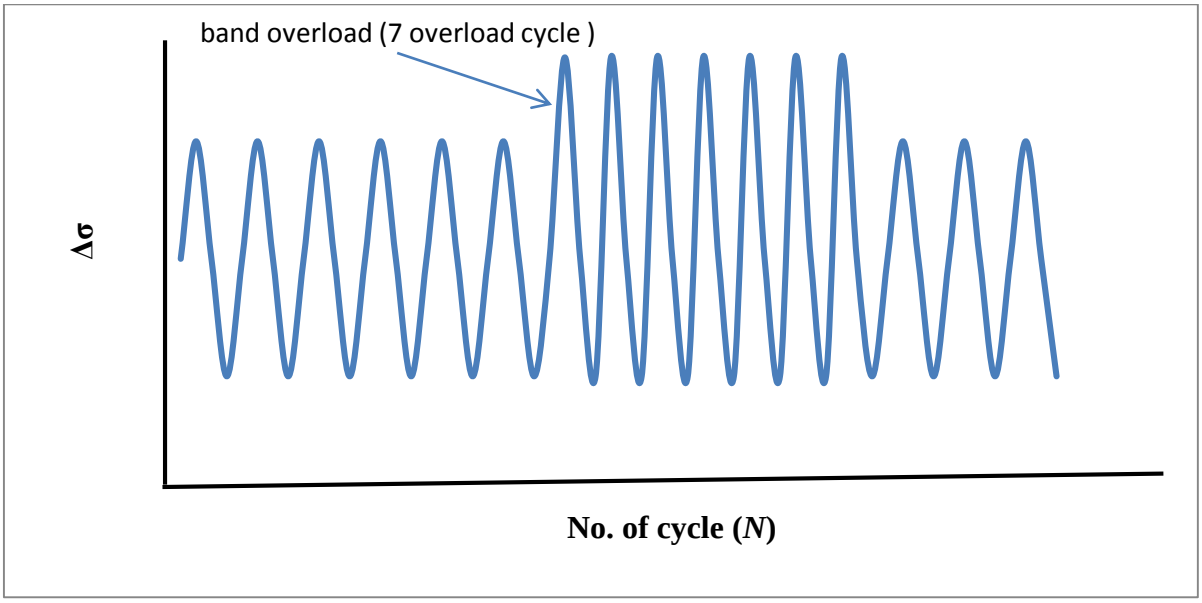

Figure. 2.11 Band overload (7 consecutive tensile overload cycle) pulses on the constant amplitude fatigue load cycle.

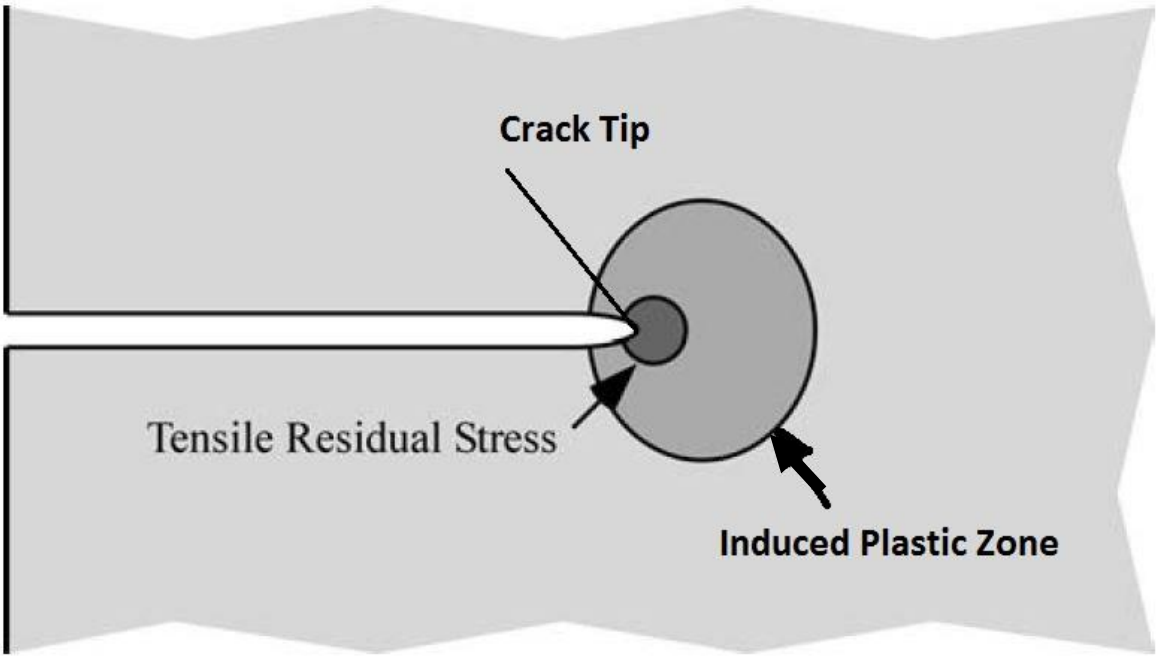

Figure 2.12 Induced plastic volumetric expansion zone at the front of crack tip during a tensile overload [4]

Chapter 3

MATERIAL, EXPERIMENT AND ANALYSIS DETAILS

MATERIAL, EXPERIMENT AND ANALYSIS DETAILS

3.1 Introduction

The Elastic plastic fracture toughness test (J_{Ic} and CTOD) at different displacement rate, and fatigue crack growth rate tests under different loading conditions on an HSLA steel. All tests were done using a 100kN, servo-hydraulic universal testing machine. Tests were on compact tension (CT) specimens under displacement control for elastic plastic fracture toughness test. The fatigue crack growth tests were done on CT-specimens under load control condition and also followed overload and different successive number of overloads (band overload) cycles on the specimens during test.

3.2. Material

The material studied in current investigation is an HSLA steel, collected from Rourkela steel plant, Rourkela. The chemical composition of material is provided in Table 3.1. This alloy has good weldability and suitable for automobile and piping industries.

Table 3.1 Chemical composition of the HSLA steel as:

Material (% wt.)	C	Mn	Si	P	S	Al	V	Nb	Mo	Fe
	0.2	1.27	0.25	0.021	0.014	0.05	0.001	0.005	0.001	balance

3.3 Metallography

3.3.1. Metallographic Specimen Preparation

For metallographic examination purpose small piece of approximately 12mm x 12mm x 10mm size were cut with the help of a hacksaw from the as-received material. The sample so cut is grinded by wheel, belt grinders and various grades of silicon carbide abrasive papers (emery papers). The specimen subsequently polished on sylvet cloth using diamond paste of particle sizes of 1μm~ 0.25μm. The metallographic specimen subsequently etched with freshly prepared 2% Nital solution.

3.3.2 Metallographic Examination

To examine the microstructure of as-received material, well etched metallographic specimens of the material were prepared in three directions: *L-T*, *L-S*, and *T-S*. Then they were examined in all three directions with the help of an optical microscope (Carl Zeiss Microscopy).

3.4 Hardness Evaluation

Hardness were examine in three directions *L-T*, *L-S*, and *T-S* surfaces with the help of a Vickers Hardness using a load of 5 kgf.

3.5 Tensile Testing

Tensile tests are performed on round bar specimens of diameter 6 mm and gauge length 30 mm out of the as received material. The tests were conducted following the ASTM standard E8-M [37]. The nominal dimensions of the tensile specimens are shown in Figure 3.1.

All tests were carried out with the help of a 100kN servo-hydraulic Universal Testing Machine connected with computer that is running Windows based monotonic application software supplied by *BiSS*. The software has facility for controlling the test control parameters, like strain rate, cross head speed and data acquisition system on load, displacement and extensometer in the channels. During test using a 25 mm gauge length extensometer at room temperature, carried out at a displacement rate 1 mm/min. The true strain was measured through 25mm gauge length extensometer, mounted to the mid-section of the specimen length.The tensile test generated data after test were investigated to estimate the various mechanical properties of the material.

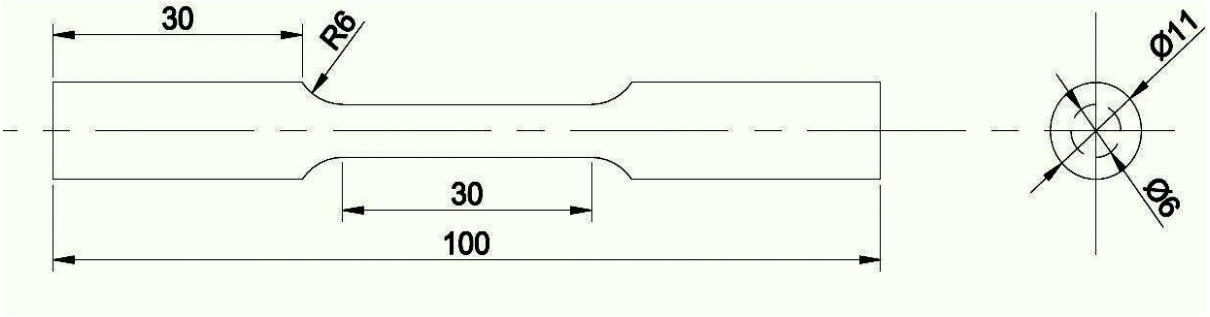

All Dimension in mm

Figure 3.1 Typical round tensile test specimen following the ASTM standard E8-M [37].

3.6 **Charpy Impact Toughness test**

Charpy impact toughness test were conducted on Indian standard specimen with dimension 10mmX10mm square cross section with 55mm length, provided 5 mm deep U-notch notched at one side at mid-point of its length. [**38**]

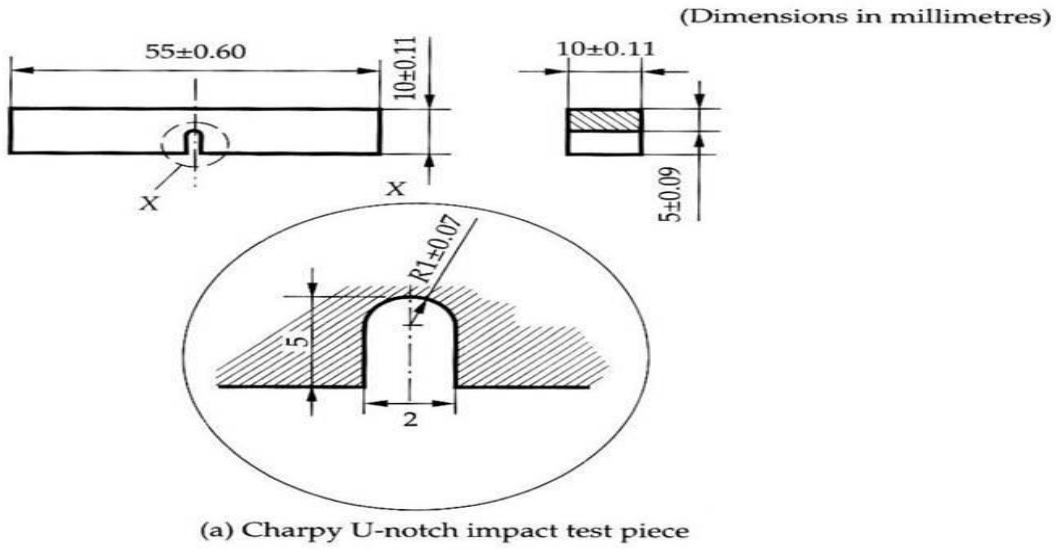

Figure 3.2 Typical U- notch charpy impact test specimen [38].

Charpy impact energy and impact toughness are determined by the following relationship as:

$$\text{Impact strength} = \frac{\text{Energy absorbed (kJ)}}{\text{Cross-sectional area at the breaking point } (m^2)}$$

3.7 Elastic plastic fracture toughness test

3.7.1 Specimen Preparation

The Elastic plastic fracture toughness tests in this research were conducted on CT specimens in *L-T* (Longitudinal- Transverse) orientation, shown in figure 3.3. Considering the available form of the material, standard 1-CT specimens with reduced thickness were machined following the guidelines of ASTM E 1820-13 [14], is shown in Figure 3.4, the specimens were fabricated such that the notch direction is transverse direction and loading direction in longitudinal direction in the *L-T* orientation with respect to the plate dimension. Typical configuration of a specimen is shown in Figure 3.4. The designed dimensions of the specimens were; thickness (B) ~12mm, width (W) is ~ 51mm and machine notch length (a_n)~9.5mm. For proper plane strain deformation and straight crack growth along the crack front, side grooves were provide with each side. The side grooving was carried out by keeping a notch angle 60 degree of to a depth of approximately 1.2 mm on each side of the specimen. This was done to enhance the stress tri-axialty at the crack tip and net thickness of specimen are around 9.4mm.The dimensions of the specimens used in this investigation are shown in Table 3.2.

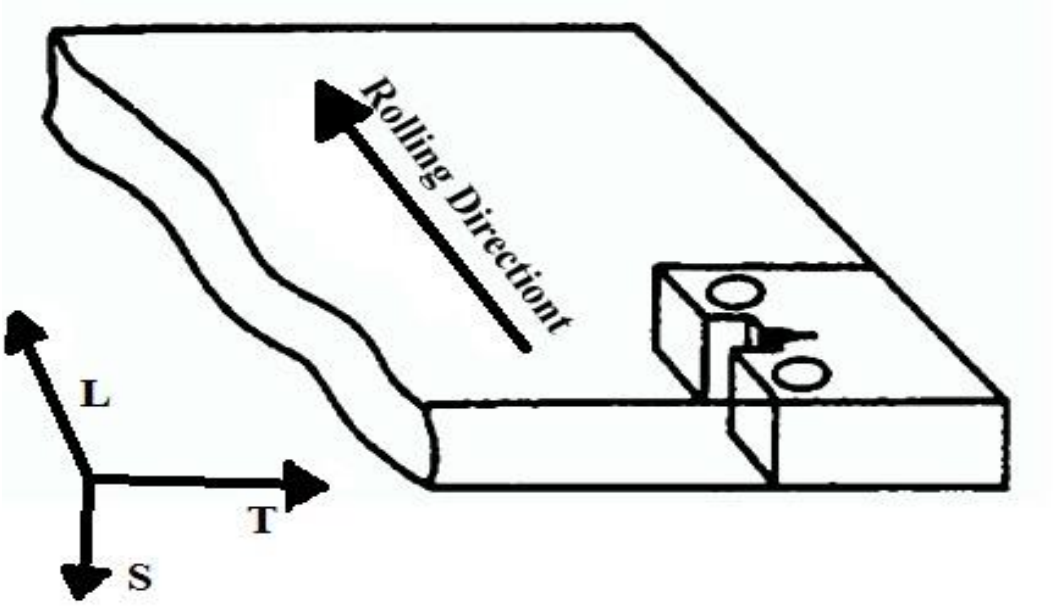

Figure 3.3 Orientation of compact tension specimens in *L-T* (Longitudinal- Transverse) direction showing with rolling direction.

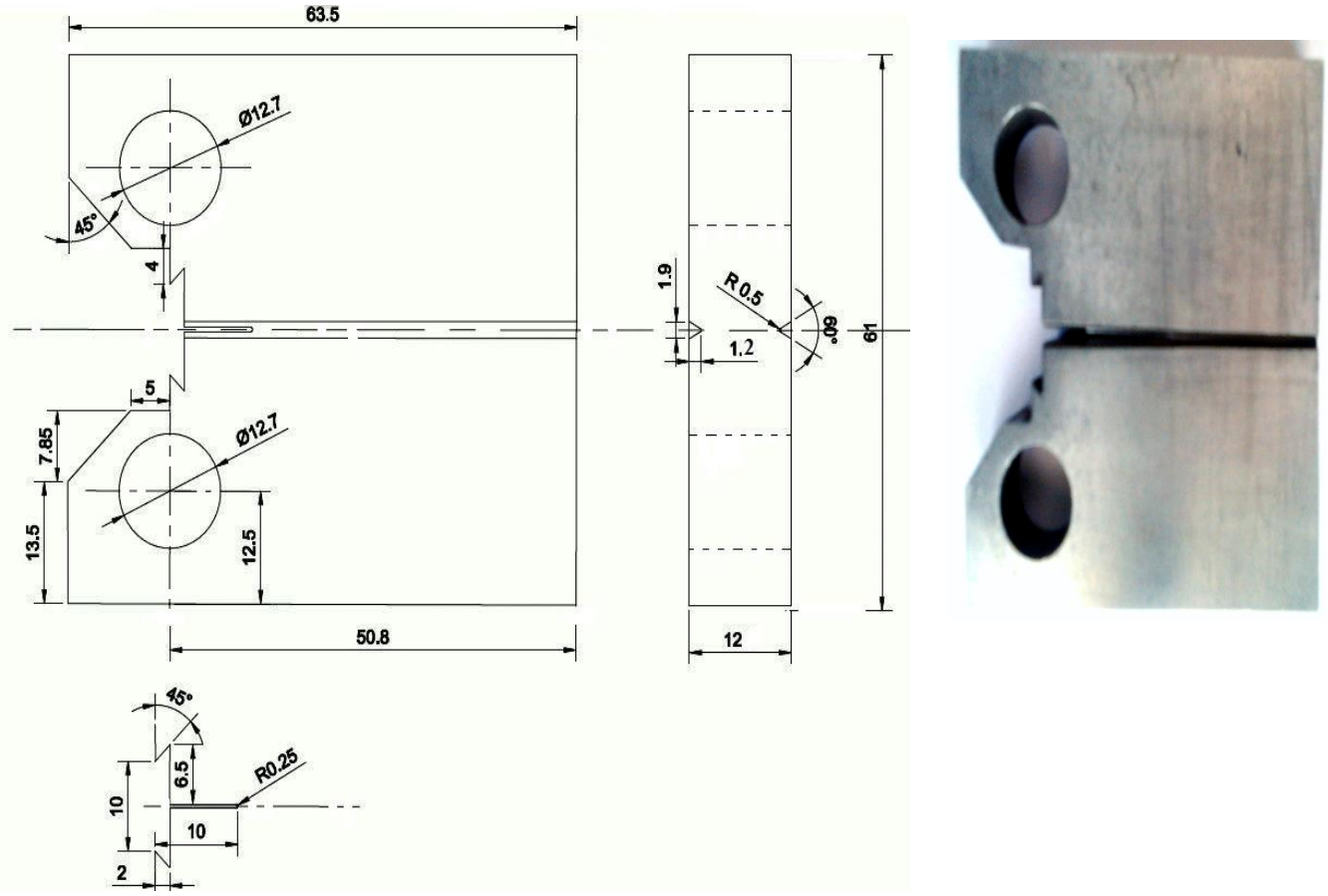

All dimensions in mm

Figure 3.4 Nominal dimensions of 1-CT specimen with notch dimensions and side grooved are provided, standard followed by ASTM- E1820-13[14].

3.7.2 *J*-Integral test

The fracture toughness tests in this investigation were done on 1-CT (compact tension) with reduced thickness specimens. J_{Ic} test had been done in two processing test steps as first on is fatigue pre crack up to a/W is 0.45 to 0.70 by ASTM-E1820-13 [14]. And second one is J_{Ic} test of pre cracked specimen, by machine each specimen were pre cracked by fatigue, to produce a very sharp initial crack. Only three typical crack length to width ratios **(**a/W) (0.45, 0.58 and 0.542) are selected and analysed in this investigation. All the pre-cracking experiments were done by computer controlled 100 kN load capacity *BiSS* servo-hydraulic universal testing machine using application software *VAFCP* (variable amplitude crack propagation) fatigue software. The software permitted on-line monitoring of the crack length (*a*), compliance, ΔK, load range and *da/dN* etc. All fatigue pre-cracking were done at a stress ratio of (*R*) 0.3 using a frequency of 10Hz and with a constant ΔK is 15 MPa$\sqrt{m}$. All load line knife edge CT specimens were pre-cracked to achieve a total crack length of approximately 26 mm, which corresponds to $\approx$ 0.45-0.6. The total crack lengths (including starter notch configuration plus fatigue pre-crack) for each specimen are given in Table 3.2. The crack length during test were measured by machine

using compliance technique with the help of *COD* gauge connected through the specimen during test.

Monotonic J-integral tests were carried out, as per the requirements of ASTM standard E1820-13 [14] on a computer controlled *100kN* capacity *BiSS* servo-hydraulic universal testing machine using *J-R Test-2370* based application software using a different displacement rate at room temperature were loading displacement was controlled. Specimens of desired crack length were loaded to the desired displacement and then unloaded it, this loading and unloading process had done up to certain termination condition followed by ASTM E 1820-13 [14]. Unloading rate were kept sufficiently slow as compared to loading rate for maintain significant linear unloading line. *J* value is calculated at several points along an unloading curve. All tests were conducted under monotonic loading conditions using of single specimen unloading compliance technique as a reference method. In this method the crack lengths are determined from elastic unloading compliance measurements. This is done by carrying out a series of sequential unloading and reloading during the test, the interruptions being made in a manner that these are almost equally spaced along the load versus displacement record. These experiments have been carried out following the ASTM E 1820-13 [14] standard. In the single specimen *J*-integral tests unloading should not exceed more than 50% of the current load value or 20% of P_m (maximum pre-crack load).

Figure 3.5 Close- up view of specimen with clevis grips and COD gauge during J_{IC} test of side grooved 1-CT specimen.

Table 3.2 Dimensions detail of the J_{Ic} Tested CT (compact tension) specimens.

Specimen ID	Specimen dimensions in mm					
	W	B	B_N	B_e	a_n	a
JIC-1	50.8	11.5	9.3	11.08	9.70	22.86
JIC-2	51	11.95	9.35	11.38	9.60	29.63
JIC-3	51	11.9	9.4	11.37	9.60	27.64

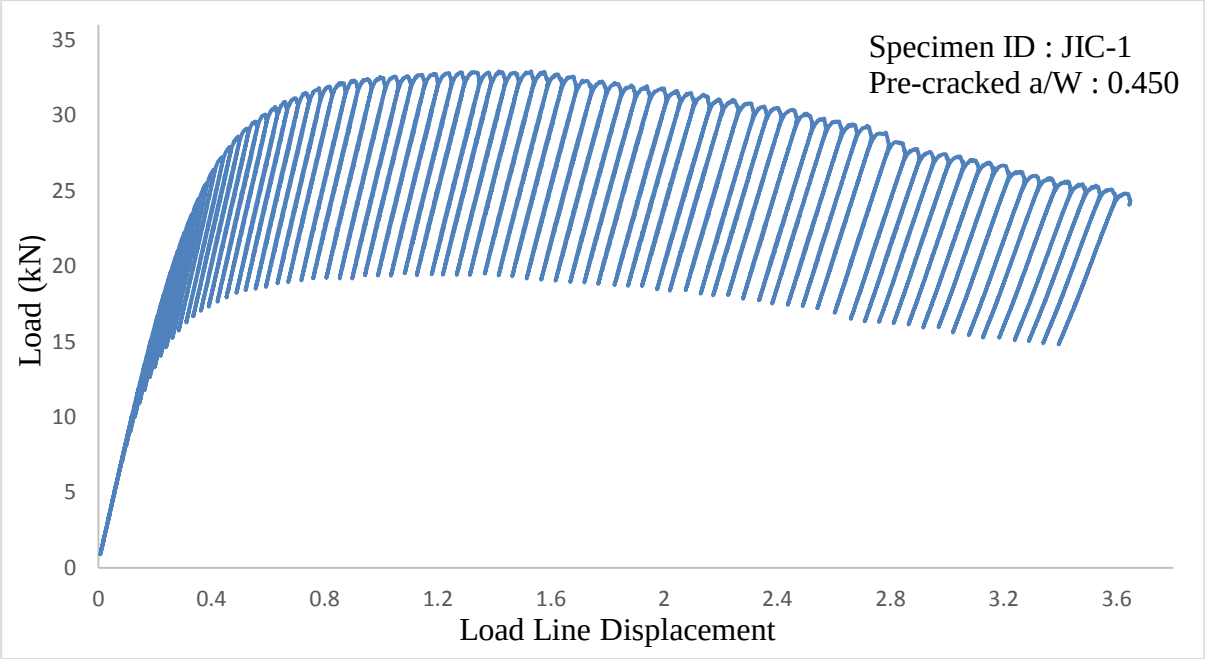

Figure 3.6 Load vs Load line displacement plot of specimen ID: JIC-1 at room temperature.

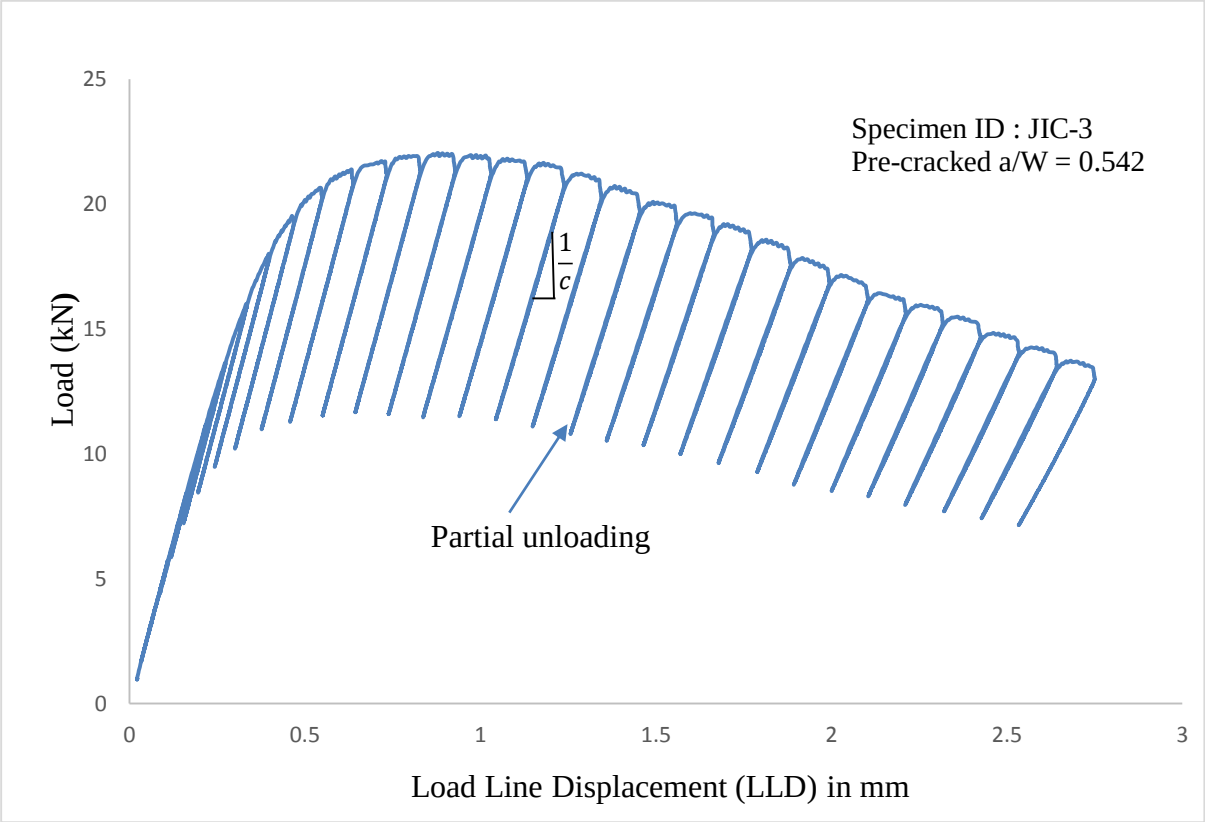

Figure 3.7 Load vs Load line Displacement plot of specimen ID: J_{IC}-3 at room temperature.

3.7.3 *J*-integral analysis detail for the Resistance curve test method according to ASTM E1820-13 [14]

Calculation of *J*-integral For the compact tension (CT) specimen at a point corresponding incremental crack length ($a_{(i)}$), incremental displacement ($v_{(i)}$), and incremental load ($P_{(i)}$) on the specimen load versus LLD plot calculate as:

$$J_i = J_{el(i)} + J_{pl(i)}$$

The magnitude of J_i is the sum of its elastic and plastic component denoted by $J_{el(i)}$ and $J_{pl(i)}$. The elastic component of $J_{el(i)}$ was calculated using the equation

$$J_{el(i)} = \frac{K^2{}_i(1-v^2)}{E}$$

And calculation of $K_{(i)}$ —For a load $P_{(i)}$, corresponding $K_{(i)}$ as:

$$K_{(i)} = \frac{P_{(i)}}{(BB_N W)^{0.5}} f\left(\frac{a_i}{W}\right)$$

Where $K_{(i)}$ is the elastic stress intensity parameter.

For calculation of $f\left(\frac{a_i}{W}\right)$ as:

$$f\left(\frac{a_i}{W}\right)=\frac{\left\{\left(2.0+\frac{a_i}{W}\right)\left[0.886+4.640\left(\frac{a_i}{W}\right)-13.320\left(\frac{a_i}{W}\right)^2+14.720\left(\frac{a_i}{W}\right)^3-5.60\left(\frac{a_i}{W}\right)^4\right]\right\}}{\left(1-\frac{a_i}{W}\right)^{1.5}}$$

Calculation of Crack Size (a_i)—From *J-R* curve analysis using unloading compliance technique, the crack size is calculate as:

$$\frac{a_i}{W}=1.000196\ -\ 4.06319u_{(i)}\ +11.242u_{(i)}{}^2-\ 106.043u_{(i)}{}^3+\ 464.335u_{(i)}{}^4-\ 650.677u_{(i)}{}^5$$

Where

$$u_{(i)}=\frac{1}{\left[B_eEC_{c(i)}\right]^{0.5}+1}$$

And $C_{c(i)}$, the crack size valuation may be modified for rotation.

Compliance is corrected as:

$$C_{c(i)}=\frac{C_i}{\left(\frac{H^*}{R}\sin\theta_i-\cos\theta_i\right)\left(\frac{D}{R}\sin\theta_i-\cos\theta_i\right)}$$

where (Figure 3.8):

C_i = measured elastic compliance of specimen (at the load line),

H* = initial half-span of the load points (centre of the pin holes),

R = radius of rotation of the crack centreline, $\frac{(W+a)}{2}$ where a is the updated crack size,

D = half of the initial distance between the displacement measurement points,

θ = angle of rotation of a rigid body element about the unbroken mid-section line, or

d_m = total measured load-line displacement.

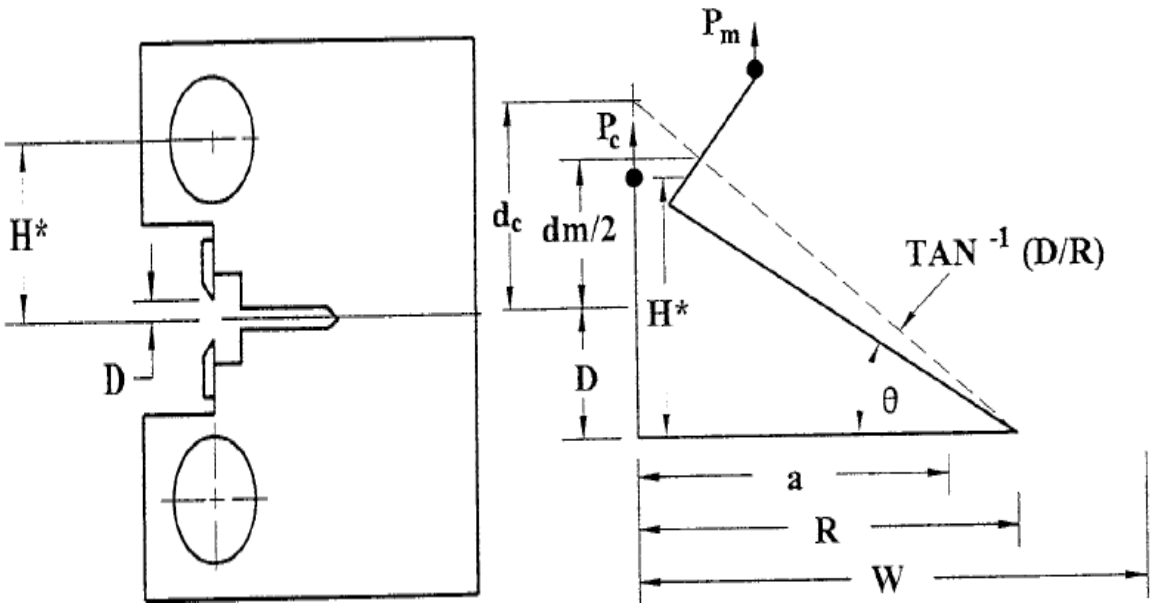

Figure 3.8 Elastic compliance correction for CT specimen rotation

And,

$$\theta_i = \sin^{-1}\left(\frac{D+\frac{d_m}{2}}{\sqrt{D^2+R^2}}\right) - \tan^{-1}\left(\frac{D}{R}\right)$$

The slope of each unloading line was calculated by linear regression analysis. The inverse of the slope is the compliance (C_i) of the specimen corresponding to the load from which the unloading has been carried out.

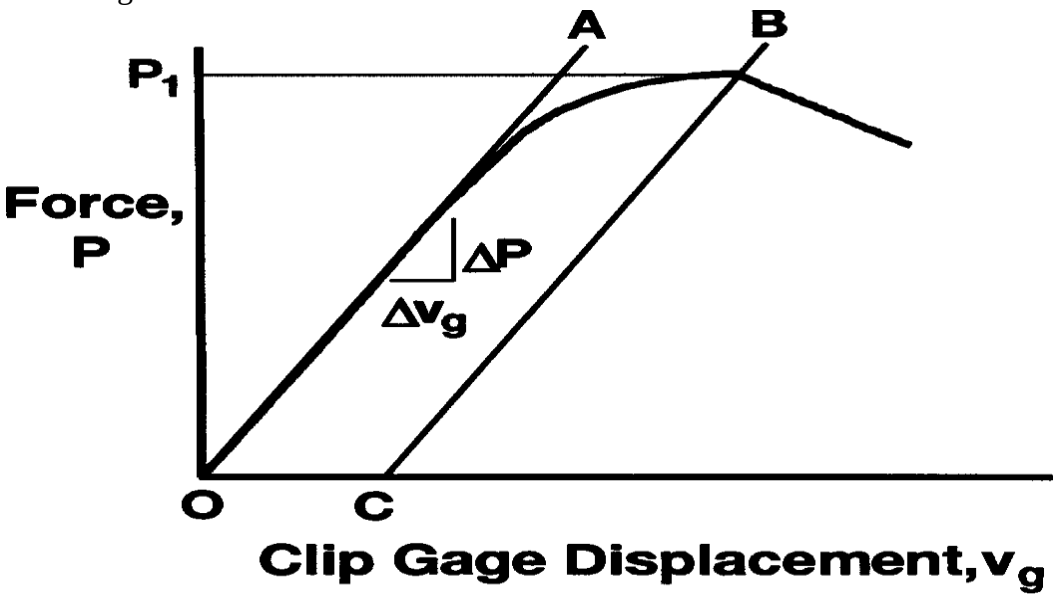

Figure 3.9 Determination of Initial Compliance.

The plastic component of $J_{pl(i)}$ were calculated using the following equation as-

$$J_{pl(i)} = \left[J_{pl(i-1)} + \left(\frac{\eta_{pl(i-1)}}{b_{(i-1)}} \right) \left(\frac{(P_i + P_{(i-1)})(V_{pl(i)} - V_{pl(i-1)})}{2B_N} \right) \right] \left[1 - \gamma_{(i-1)} \left(\frac{a_i - a_{(i-1)}}{b_{(i-1)}} \right) \right]$$

Where-

$$\eta_{pl(i)} = 2.0 + 0.5220 \frac{b_{(i-1)}}{W}$$

and

$$\gamma_{(i-1)} = 1.00 + 0.760 \frac{b_{(i-1)}}{W}$$

Where-

$V_{pl(i)}$ = plastic portion of the LLD, and

$V_{pl(i)} = V_i - P_i C_{LL(i)}$

and

$C_{LL(i)}$ = experimental compliance, $\left(\frac{\Delta V}{\Delta P} \right)_i$ corresponding to the current crack size, a_i.

An experimental elastic compliance, $C_{LL(i)}$, calculated from the following equation:

$$C_{LL(i)} = \frac{1}{EB_e} \left(\frac{W + a_i}{W - a_i} \right)^2 \left[2.1630 + 12.219 \left(\frac{a_i}{W} \right) - 20.065 \left(\frac{a_i}{W} \right)^2 - 0.9925 \left(\frac{a_i}{W} \right)^3 + 20.609 \left(\frac{a_i}{W} \right)^4 - 9.9314 \left(\frac{a_i}{W} \right)^5 \right]$$

Where-

$$B_e = \left[B - \frac{(B - B_N)^2}{B} \right]$$

Plotting procedure of *J-R* Curve:

The *J*-integral values (J_i) and the equivalent crack length (a_i) values were plotted as shown in figure 3.10, and cubic fit of valid data region for finding intercept value of the fitted curve and this is the value of a_{oq}. If an elastic unloading compliance technique is used, modification the *J-R* curve according to the process for each a_i value, calculate a corresponding Δa_i as follows:

$$\Delta a_i = a_i - a_{oq}$$

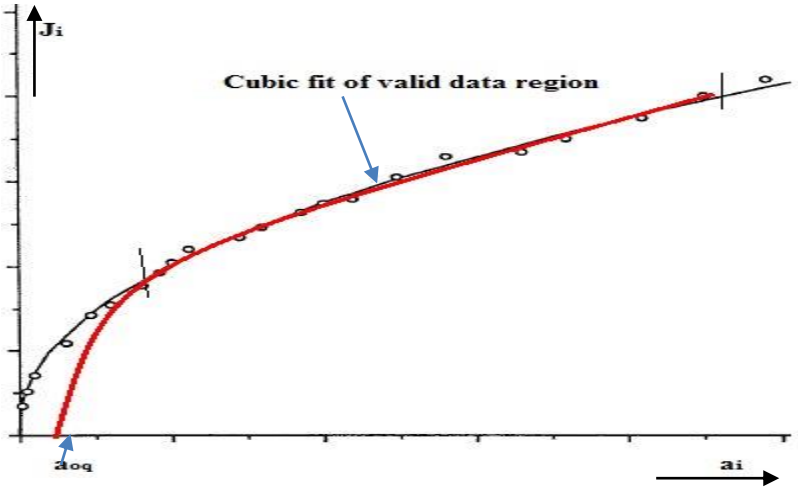

Figure 3.10 Cubic fit of valid data region in J_i vs a_i curve

Plot *Ji* versus *Δai* as shown in Figure 3.11. Draw a construction line according to the following equation:

$$J = 2\sigma_Y \Delta a$$

According to above equation draw the construction line, after that plot an 0.15 mm exclusion line parallel to the construction line intersecting the abscissa at 0.15 mm. Plot a second 1.5mm exclusion line parallel to the construction line intersecting the abscissa at 1.5 mm. Plot all $J - \Delta a$ data points that fall inside the area enclosed by these two parallel lines and covered by limit value of J and that shows as-

$$J_{limit} = \frac{b_o \sigma_Y}{7.5}$$

- Plot a 0.2mm offset line parallel to the construction and exclusion lines intersecting the abscissa at 0.2 mm.
- Using the least squares method for determining a power regression line of the following form:

$$\ln J = \ln C_1 + \ln C_2 \ln \frac{\Delta a}{k}$$

The load vs. load line displacement (LLD) data obtained from the tests were analysed to compute the magnitude of crack extension (Δa_i) and the corresponding J_i integral value at each unloading sequence as shown in fig. 3.11.

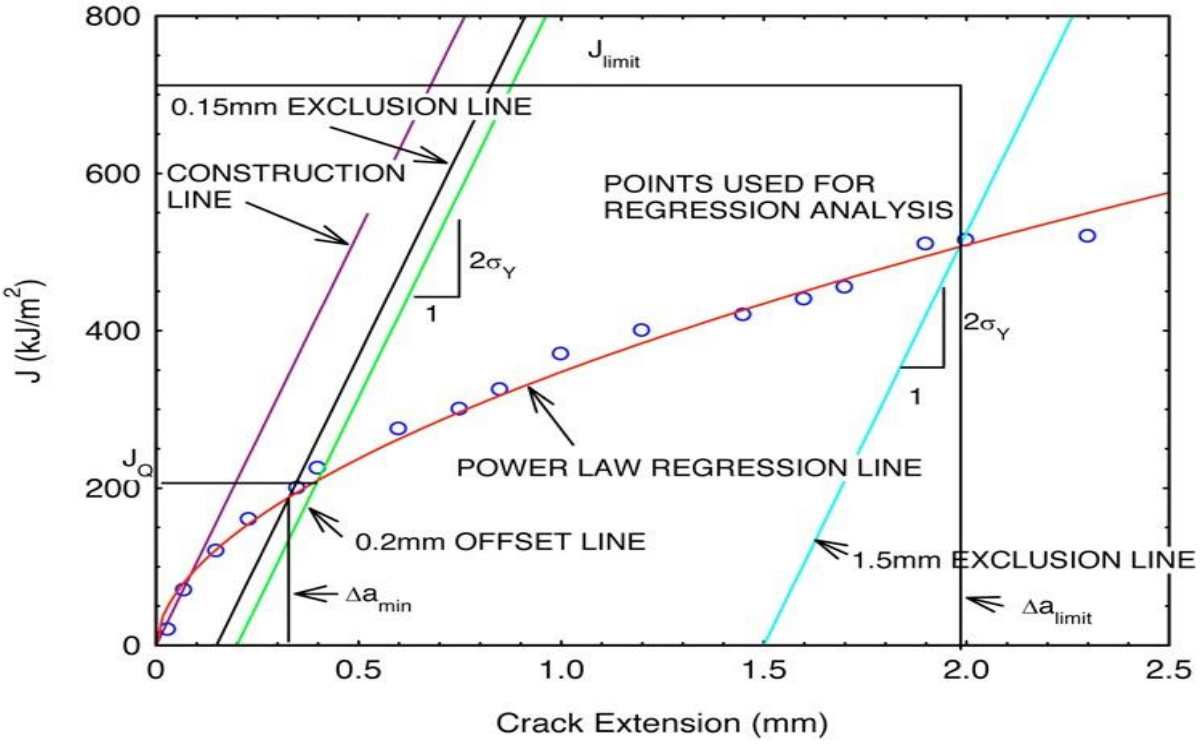

Figure 3.11 Definition of construction lines for data qualification

Qualification of J_Q as J_{Ic}

a size independent value of fracture toughness $J_Q = J_{Ic}$, if:

Thickness and Initial ligament fulfil the validity criteria

$$B, b_0 > \frac{10 J_Q}{\sigma_Y}$$

Evaluation of K_{JIc} as:

$$K_{JIc} = \sqrt{\left(\frac{E J_{Ic}}{(1-\nu^2)}\right)}$$

3.7.4 Analysis of CTOD by δ-*R* curve test method—

Form this method, calculations of CTOD for any point on the force-displacement curve are calculate from the relation as shown below:

$$\delta = \frac{J_i}{m\sigma_Y}$$

And where

$$m = A_0 - A_1\left(\frac{\sigma_{YS}}{\sigma_{TS}}\right) + A_2\left(\frac{\sigma_{YS}}{\sigma_{TS}}\right)^2 - A_3\left(\frac{\sigma_{YS}}{\sigma_{TS}}\right)^3$$

With: A_0=3.62, A_1 = 4.21, A_2=4.33, and A_3=2.00. For calculation of δ_i requires $\left(\frac{\sigma_{YS}}{\sigma_{TS}}\right) \geq 0.5$.

The maximum δcapacity for a specimen is given asfollows:

$$\delta_{\max} = \frac{b_0}{10m}$$

Construction of δ-*R* curve

The δ_i values and the corresponding crack extension Δa_i values were plotted as δ-*R* curve. The procedure for construction of δ-*R* Curve is same as *J*-*R* curve. Some value is different from *J*-*R* curve during construction of δ-*R* Curve as:

Firstly plot Plot δ_i versus Δa_i , Draw a construction line by using the following equation:

$$\delta_i = 1.4\,\Delta a_i$$

for δ_{limit} is calculate as:

$$\delta_{limit} = bo / 7.5m,$$

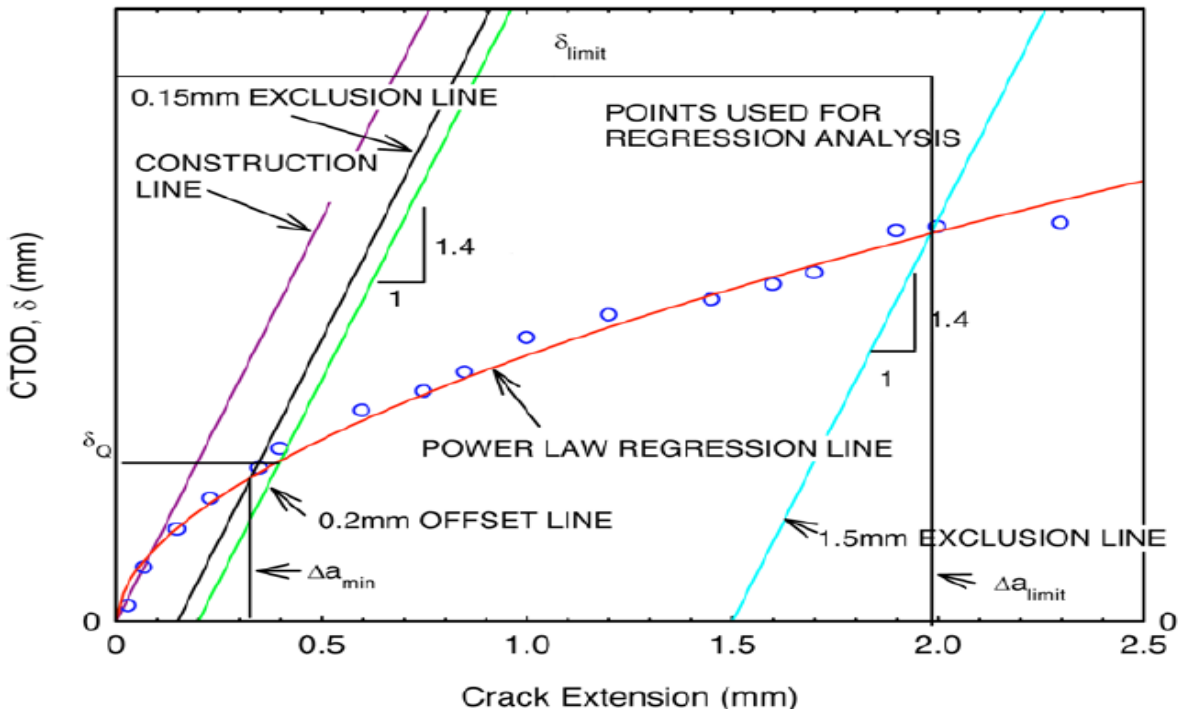

Figure 3.12Definition of Construction Lines for Data Qualification

Qualification of δ_q as δ_{Ic} : a size-independent value of fracture toughness, $\delta_Q = \delta_{Ic}$, if:

The initial ligament, $b_o \geq 10m\delta_Q$

3.8 Fractography of J_{Ic} tested fracture surface

Approximately 12 mm long parts of samples were cut from the fractured surface of tested specimen for fractographic examinations. The specimen parts were selected as the parts having contained as fatigue pre-cracked and the fractured surface. The fractured surfaces were well cleaned by ethenol and were examined with the help of a field emission scanning electron microscopy (*FESEM*). The various images taken by *FESEM* at different magnitude and resolution for proper understanding the fracture behaviour of the material.

3.9 Fatigue Crack Growth Test

3.9.1 Test Specimen geometry

Fatigue crack growth tests, were conducted on CT (Compact Tension) specimens with a narrow notch and reduced thickness, which is fabricated from 12 mm thick plate. The CT specimens were made in the L-T orientation, both sides of the specimen surfaces were given mirror-polish with the help of different grades of emery papers with the loading aligned in the longitudinal direction and notch given in the transverse direction, standard ASTM E647-13 [39] are followed for specimen geometry design. The dimensional details of specimen are presented in Figure 3.13.

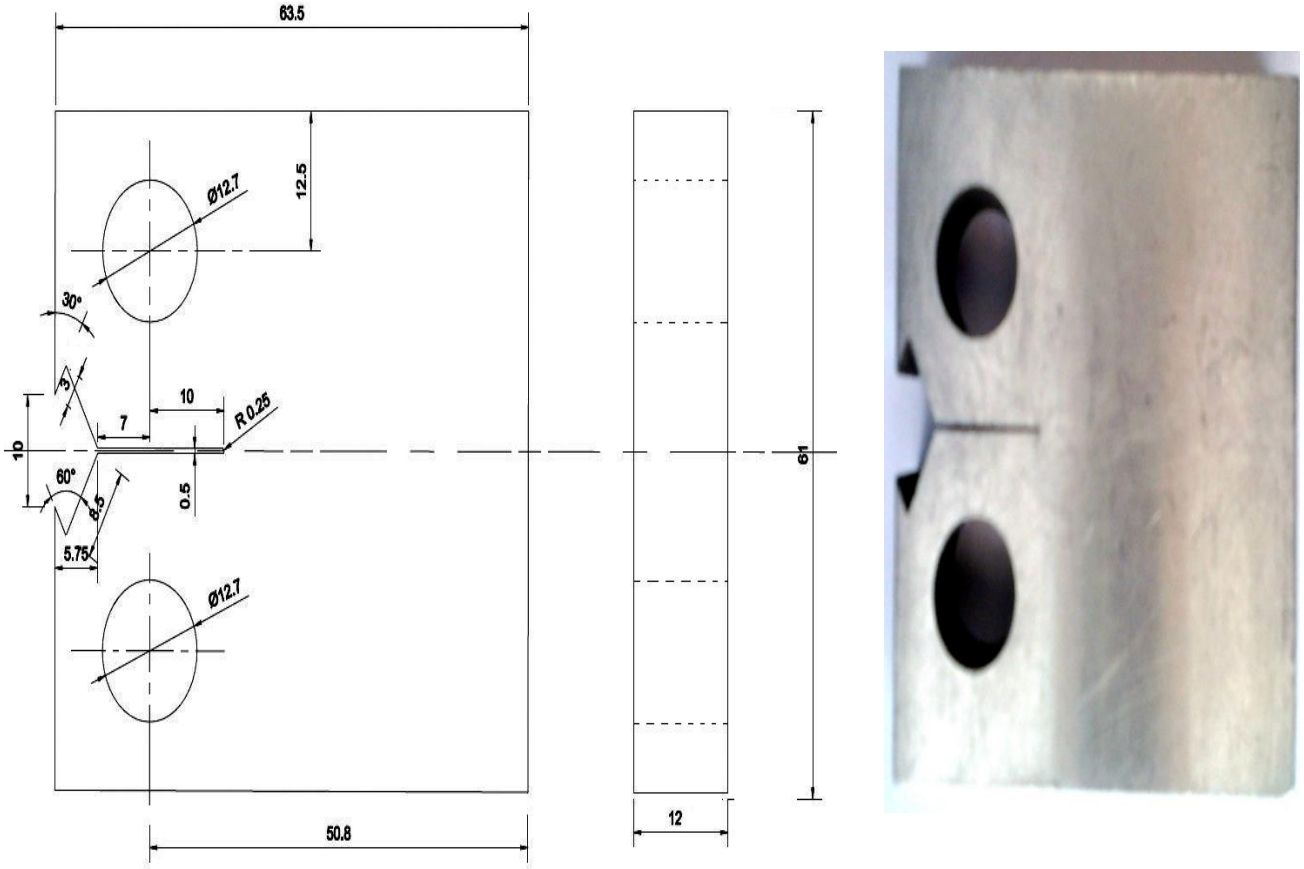

All dimensions in mm

Figure 3.13 Compact tension (CT) Specimen geometry (LT orientation) followed by ASTM E 647-13 [39]

3.9.2 Test equipment

The machine used for the fatigue crack growth tests was a computer controlled *BiSS* servo-hydraulic universal testing machine having 100 kN load capacity using *VAFCP* (variable amplitude crack propagation) fatigue application software.

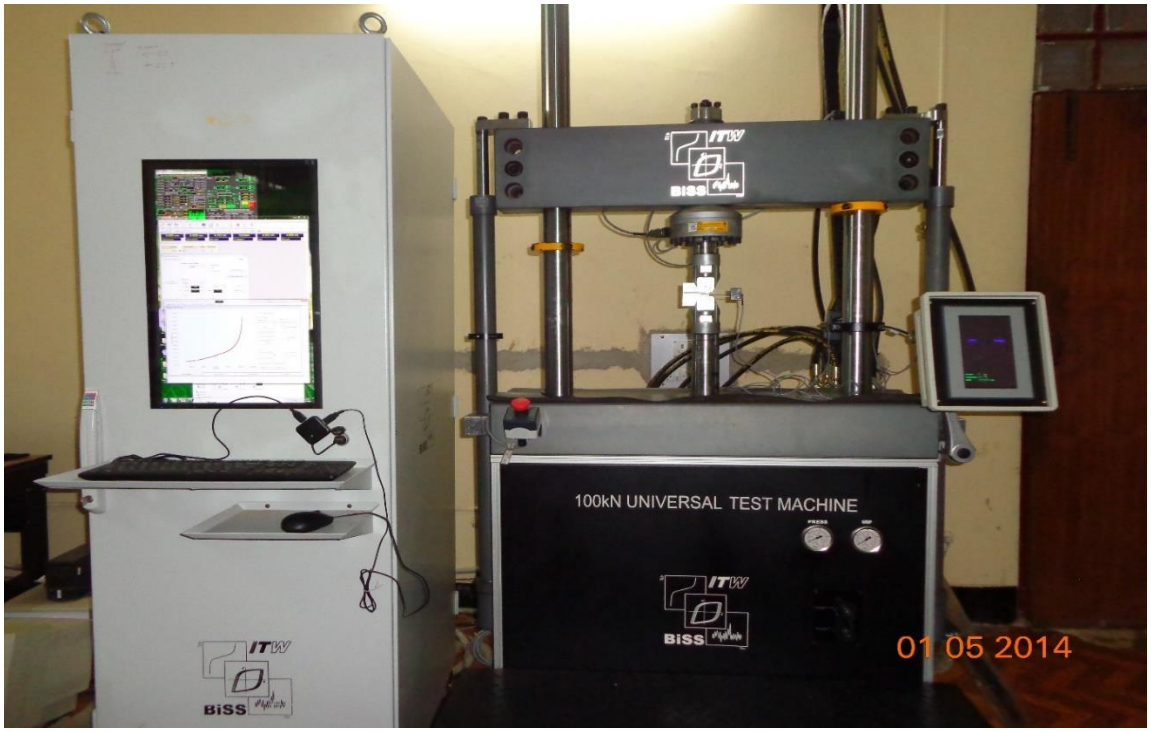

Figure 3.14 Overall arrangement to conduct fatigue crack growth test with specimen held in clevis grips during test by computer controlled 100kN load capacity BiSS Universal test machine (UTM).

3.9.3 Test program

Computer controlled 100kN load capacity *BiSS* Universal test machine *(*UTM*)* using *VAFCP* (variable amplitude crack propagation) fatigue software.The software permitted on-line monitoring of the crack length (a), compliance, ΔK, load range and the crack growth rate per cycle, (*da/dN).* All test were conducted at constant load mode at stress ratio of (*R*) 0.3 and using 10Hz frequency. For fatigue crack growth test were perform on CT specimens in accordance with ASTM E647-13 [39]. This test program runs under a room temperature. The *VAFCP* application software are used program has the ability to use the compliance method to measure crack length with the help of a *COD* gauge.

3.9.4 Fatigue crack growth tests

The specimen surfaces were stick by graph paper for manually examine the crack extension during the test as well. The *COD* gauge was mounted on the knife edges of specimen to monitor crack extension by software based program. Fatigue pre-cracking was done under mode-I loading (crack opening mode) at constant amplitude loading mode to an *a/W* ratio of 0.24. Following three different case of crack growth tests were performed in this investigation:

(i) Constant amplitude loading with constant stress ratio (*R*).
(ii) Constant amplitude loading with single overload in mode-I.
(iii) Constant amplitude loading with band (multiple) overload in mode-I.

When the tests were conducted in constant load control mode (i.e. increasing ΔK with crack extension), using a Computer controlled *BiSS* 100kN load capacity servo-hydraulic dynamic universal testing machine (UTM) (shown in figure 3.12). All the three sets of tests were done in ambient temperature condition at a frequency of 10 Hz and load ratio (*R*) of 0.3.
For determining of the stress intensity factor range (ΔK) [39] for CT specimen were calculated by following equation:

$$\Delta K = \frac{\Delta P}{B\sqrt{W}} \frac{(2+\alpha)}{(1-\alpha)^{1.5}} \left(0.886 + 4.64\alpha - 13.32\alpha^2 - 14.72\alpha^3 - 5.6\alpha^4\right)$$

Where $\alpha = \frac{a}{W}$; expression valid for $\frac{a}{W} \geq 0.2$

3.9.4.1 Constant amplitude load test

In case-(i) - CT specimens were tested under constant amplitude load mode maintaining a fixed load ratio, $R = 0.3$.
In case- (ii) - CT specimens were tested under same loading conditions with single tensile overload are applied in mode-I at, $\frac{a}{W} = 0.28$, with overload ratio (R_{ol}) were applied 1.25, in 1 Hz frequency.

The overload ratio is $R_{ol} = \frac{K_{ol}}{K^B_{max}}$

Where, K_{ol} is over load stress intensity factor, and K^B_{max} is the maximum stress intensity factor for base line test. The specimens were subsequently subjected to mode-I constant amplitude load cycles after overload.

In case- (iii) constant amplitude loading with band (multiple) tensile overload were applied in mode-I, approximately same size and dimensions, CT specimens were tested in order to investigate the effect of a band overload in mode-I

After band overload on the subsequent constant amplitude fatigue crack growth test were allowed for continue the test. The crack was allowed to grow up to , $\frac{a}{W} = 0.67$. Band-overload tests ware followed by multiple tensile overload at $\frac{a}{W} = 0.28$, and overload ratio (R_{ol}) were applied 1.25, in 1 Hz frequency. The number of band overload were applied during test are 3, 5,7,10,100, in the same crack opening mode.

The experimental parameters for all the tests are mentioned in Tables 3.3 and 3.4 respectively.

Tables 3.3 experimental parameters for constant amplitude loading test.

P_{max} (kN)	P_{min} (kN)	R	a_o (mm)	a_f (mm)	f (Hz)
11.8	3.54	0.3	11	34.34	10

Table 3.4 various experimental parameter that were used during the test of specimens under mode-I single and band overload

P_{max} (kN)	P_{min} (kN)	P_{max}^{ol} (kN)	R	R_{ol}	$(\frac{a}{W})_{ol}$	a_o (mm)	a_{ol} (mm)	a_f (mm)	f_{ol} (Hz)	f (Hz)
11.8	3.54	14.75	0.3	1.25	0.28	11	14.154	34.00	1	10

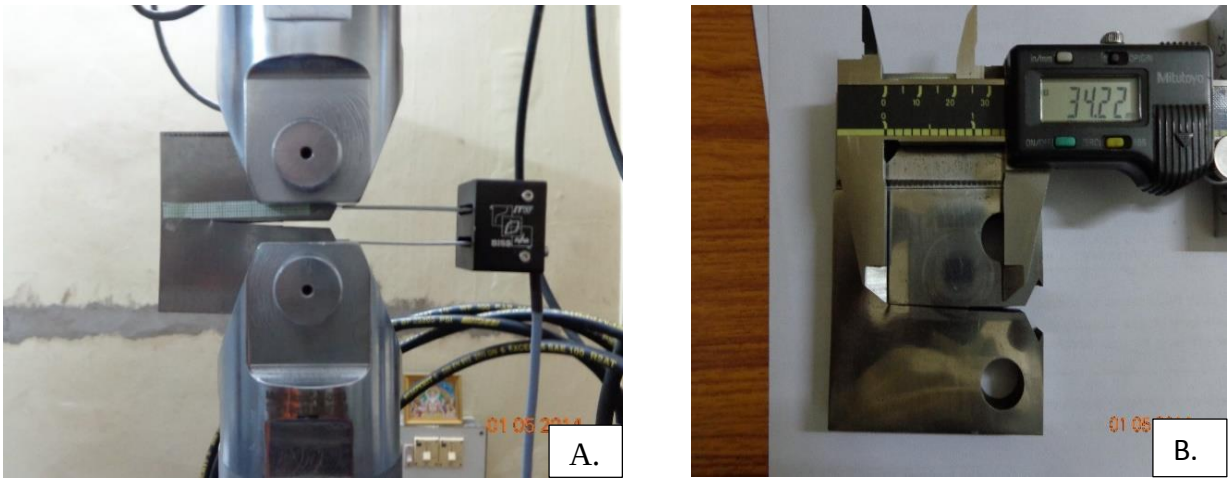

Figure 3.15 (A.) experimental setup of specimen with COD gauge during test;
(B.) Measurement of crack length by Vernier calipers after test.

3.10 Fractography of fatigue fracture surface

Approximately 12 mm long parts of samples were cut from the fractured surface of fatigue crack growth tested specimen for fractographic examinations. The specimen parts were selected as the parts containing as fatigue crack propagated parts for constant amplitude loading specimen and for 7 cycle Overloading specimen containing as the zone as before and after overloading portion with overloading zone The fractured surfaces were well cleaned by ethanol and were examined with the help of a field emission scanning electron microscopy (*FESEM*). The various images taken by *FESEM* at different magnitude and resolution for proper understanding the fracture behaviour of the material.

Chapter 4

RESULTS AND DISCUSSIONS

4.1 Introduction

The characterisation of microstructural feature, phase and mean grain size analysis, is described in section 4.2 to 4.4. Basic mechanical properties of as-received material are discussed in section 4.5.Fracture toughness test related results and tested fracture surface fractography are discussed in section 4.6 and 4.7 respectively. Fatigue crack growth rate test results and tested fracture surfaces fractography deals on section 4.8 and 4.9 respectively.

4.2 Microstructural analysis

Well-polished and etched metallographic specimens were studied using an optical microscope (Carl Zeiss Microscopy). Typical optical micrographs of as-received material are illustrated in Figure 4.1. The white portion of microstructure refers to ferrite and light black portion refers to pearlite. The dark black portion appears as martensite along with carbide precipitate throughout structure in this steel. The ferrite matrix gives ductility and toughness to the investigated steel.This optical microstructure illustrates the alignment and grain structures of the rolled plate in three mutually orthogonal directions. The microstructures of all three directions were superimposed to obtain the 3-D view and shown in Figure 4.1.

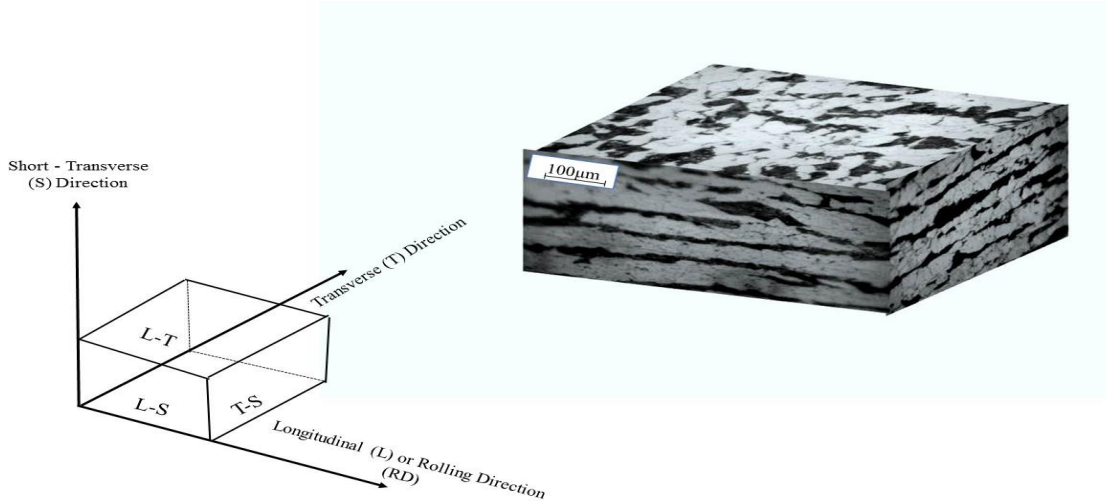

Figure 4.1 Triplanar optical micrograph of as-received material, etched by 2% Nital.

4.3 Phases and grain size analysis

Phase analysis of as-received material were investigated by Carl Zeiss Microscopy and is shown in Figure 4.2. The alloy contents 62 % ferrite, 31% pearlite and 7% martensite along with carbide precipitates. However identification of martensite and carbide precipitates need TEM analysis. Mean grain size distribution is found as 15.417µ by taking average of three consecutive reading from Microscopy using ASTM E 1382 for grain size analysis.

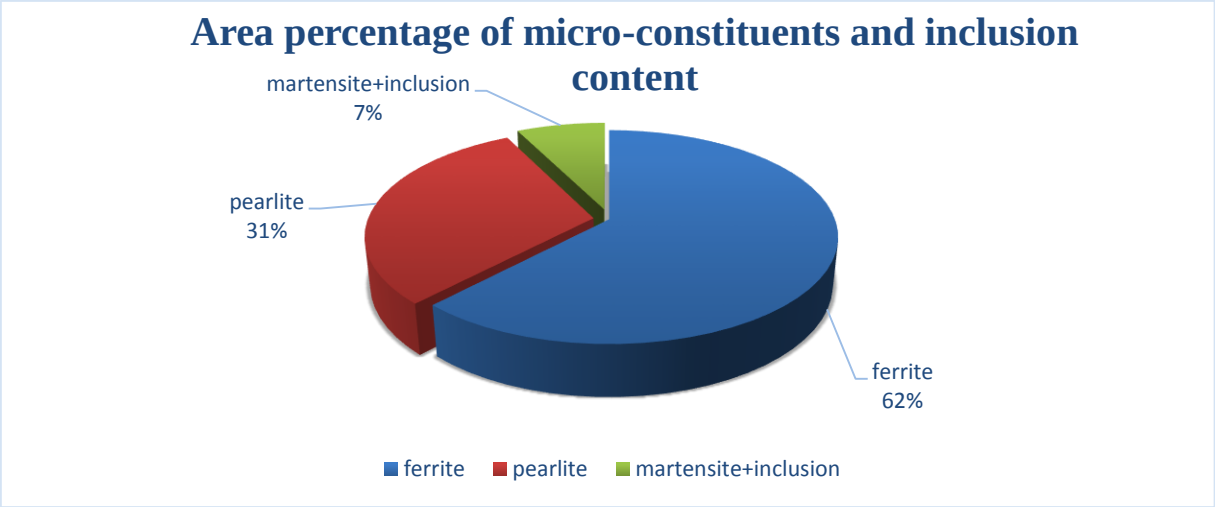

Figure 4.2 Area percentage of micro-constituents and inclusion content on microstructure

4.4 EDS analysis

To determine the elements present in as-received material, EDS analysis is done. EDS spectrum of investigated samples are shown in Fig.4.3.

From that figure it was observed that in the steel contents large amount of Mn and micro-alloying elements, Mo, Nb and V.

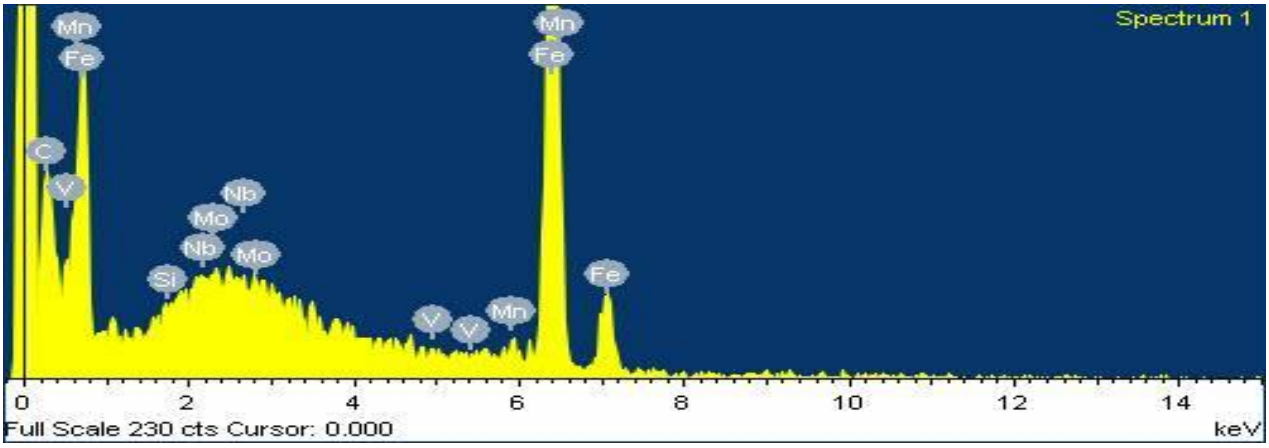

Figure 4.3 EDS analysis of material by SEM.

4.5 Basic mechanical properties analysis

4.5.1 Hardness

Hardness values were measured in all three perpendicular directions e.g., L-T, L-S and T-S surfaces with the help of a Vickers Hardness Testing machine applying a load of 5 kgf. For each surface five indentations were taken to get mean value of hardness of the steel.
The hardness data in all three directions are shown in Figure 4.4.

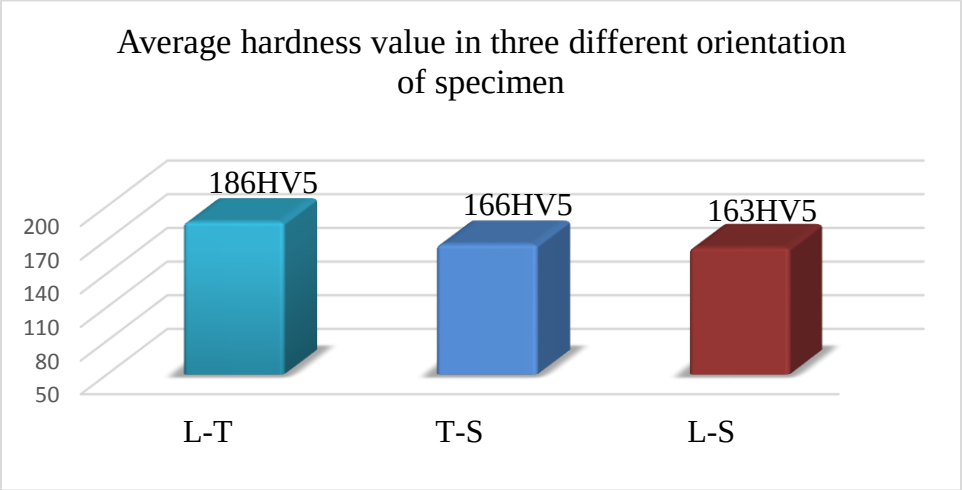

Figure 4.4 Hardness values of steel in three different orientation

4.5.2 Tensile properties

The tensile tests were conducted and the engineering stress-strain plot and true stress-strain plot are shown in Figure 4.5 and 4.6 and the tensile properties in Table 1. The tensile values are taken by the average of two test. The 0.2% yield stress and ultimate tensile stress values from the two tests are showed almost same.

Table 4.1 Tensile properties of HSLA steel

Material	σ_{YS} (MPa)	Yield Load (kN)	σ_{UTS} (MPa)	Peak Load (kN)	E (GPa)	Poission ratio (υ)	Strain Hardening exponent (n)	Strain Hardening Co-efficient (K) (MPa)	% Elongation in 25mm gauge length	% Reduction in Area
HSLA steel	622.45	17.69	778.62	22.22	210	0.33	0.156	1439.65	27	47.9

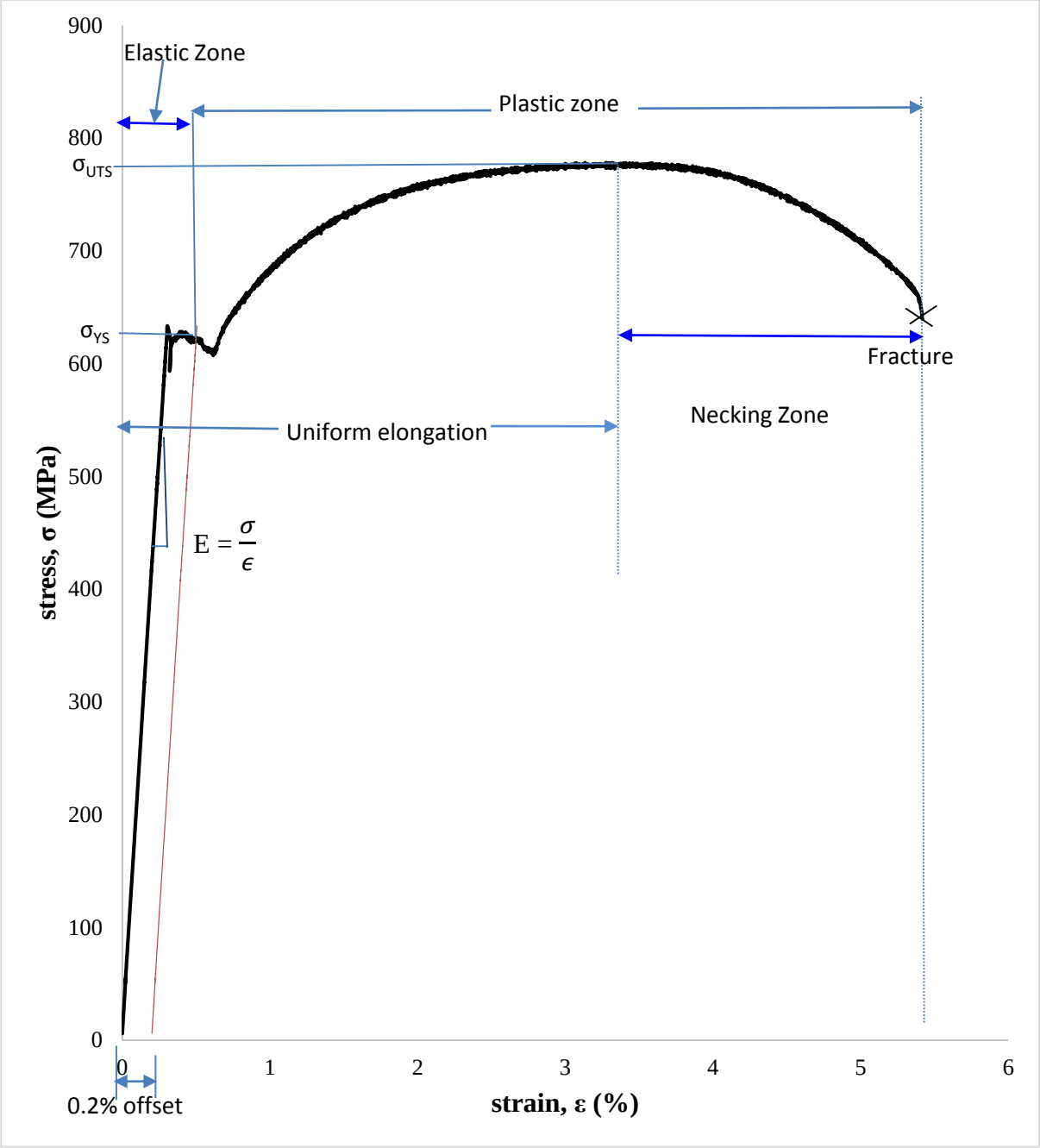

Figure 4.5 Typical engineering stress-strain curve obtained from a tensile test of HSLA steel at room temperature, showing with various features

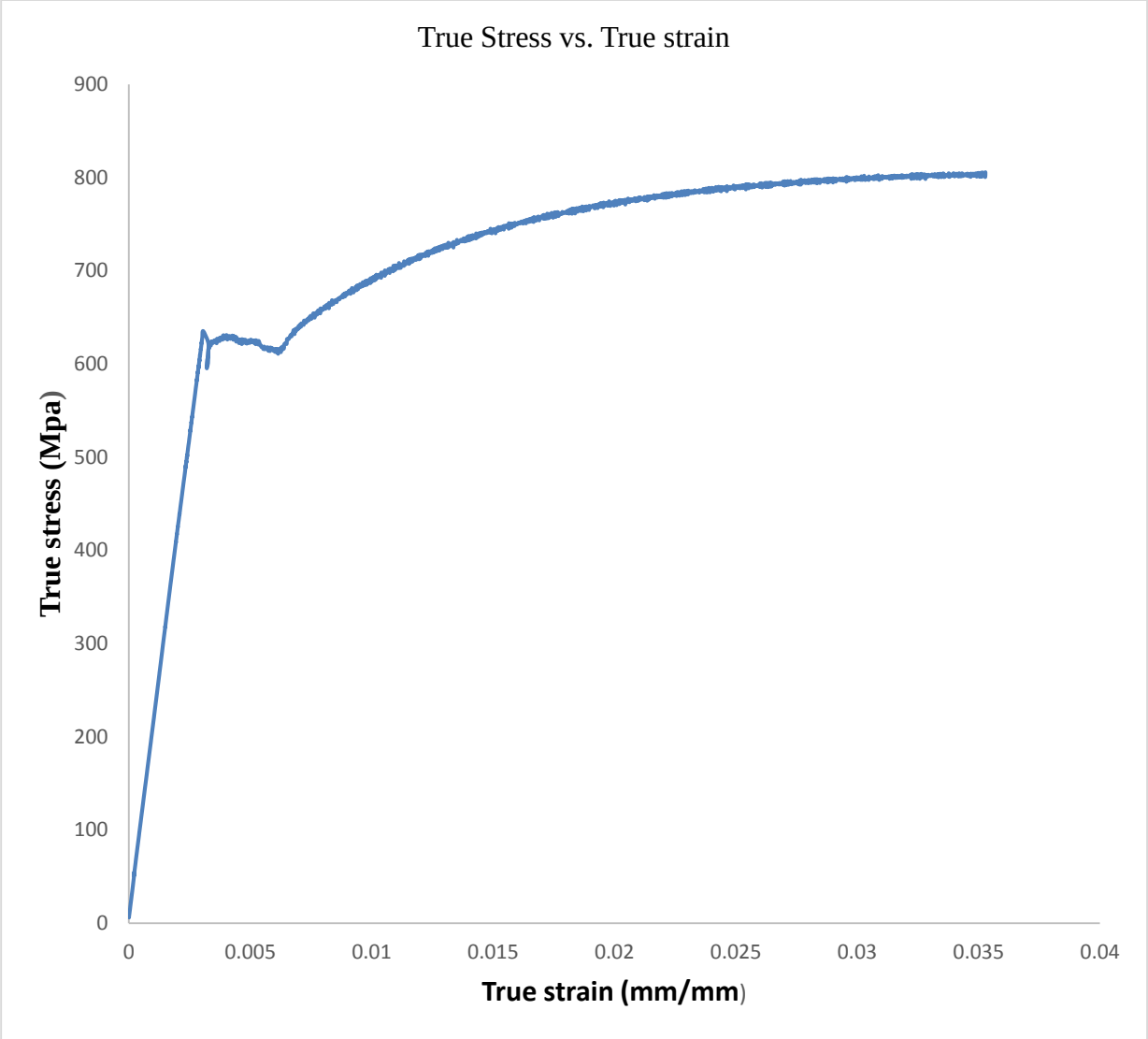

Figure 4.6 Typical true stress-strain curve obtained from a tensile test of an HSLA steel at room temperature.

4.5.3 Charpy impact test property

Charpy test were conducted using a U-notched specimens. And impact energy and impact toughness of an HSLA steel after calculatin found as:

Table 4.2 Charpy impact test property

Material	Impact energy (J)	Impact toughness $\left(\frac{kJ}{m^2}\right)$
HSLA steel	67.52	1125.3115

4.6 Elastic plastic fracture toughness (J_{Ic} and δ_{Ic})

Experimental *J*-integral and CTOD results of as-received steels as J_{Ic} and δ_{Ic} are shown in figure 4.7 to 4.9, and figure 4.11 to 4.13 as a function of crack extension Δa for displacement rates 0.03, 0.05 and 0.1mm/s using specimens of same thickness, results show from figure 4.10 and 4.14 that specimen ID: JIC-2 has maximum value of fracture toughness which is conducted at 0.03 mm/s displacement rate. The estimated *J*-integral fracture toughness values of the steel at room temperature is decreases with increasing displacement rate all the results related resistance curve and table shown below.

4.6.1 *J*- integral fracture toughness (J_{Ic})

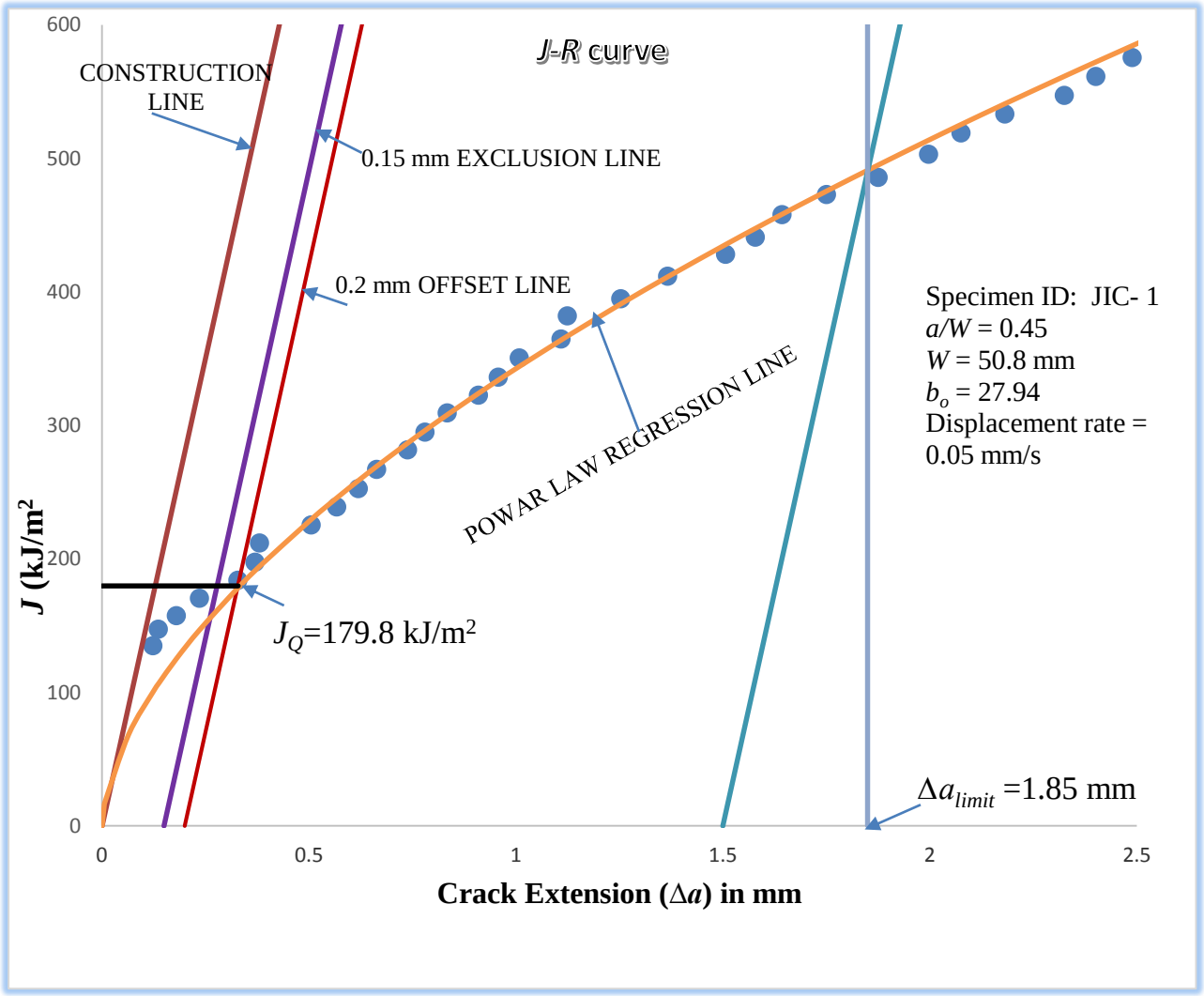

Figure. 4.7 Typical *J-R* curve of specimen ID: JIC-1 at room temperature.

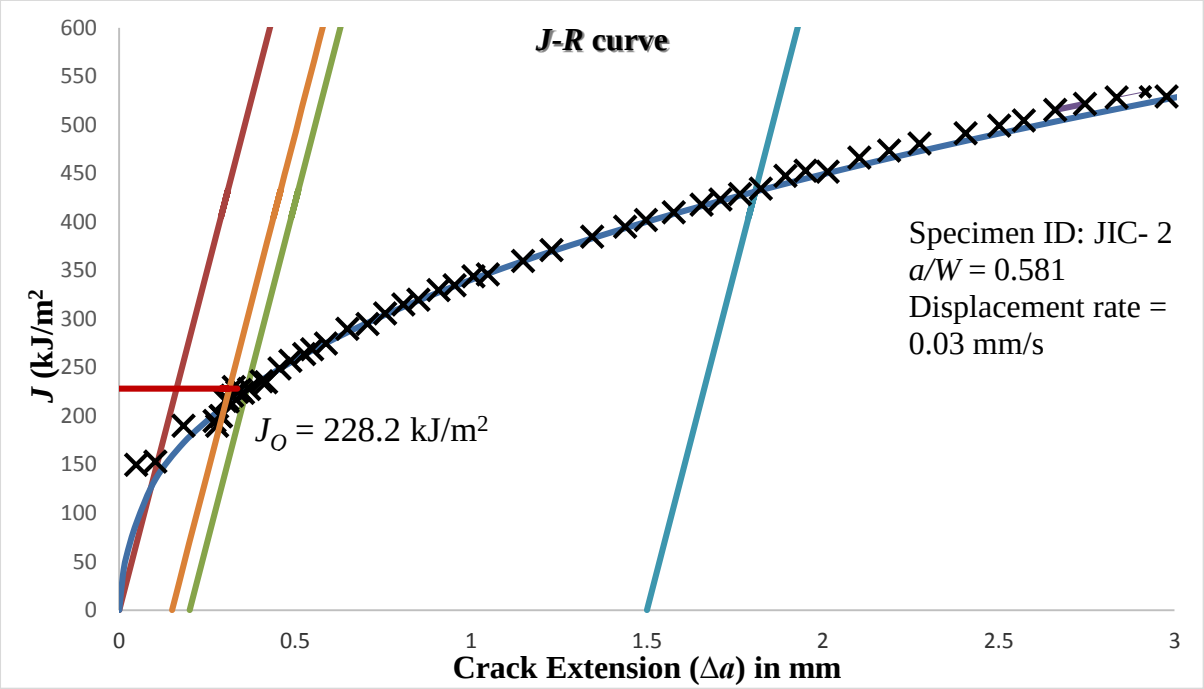

Figure 4.8 Typical *J-R* curve of specimen ID: JIC-2 at room temperature.

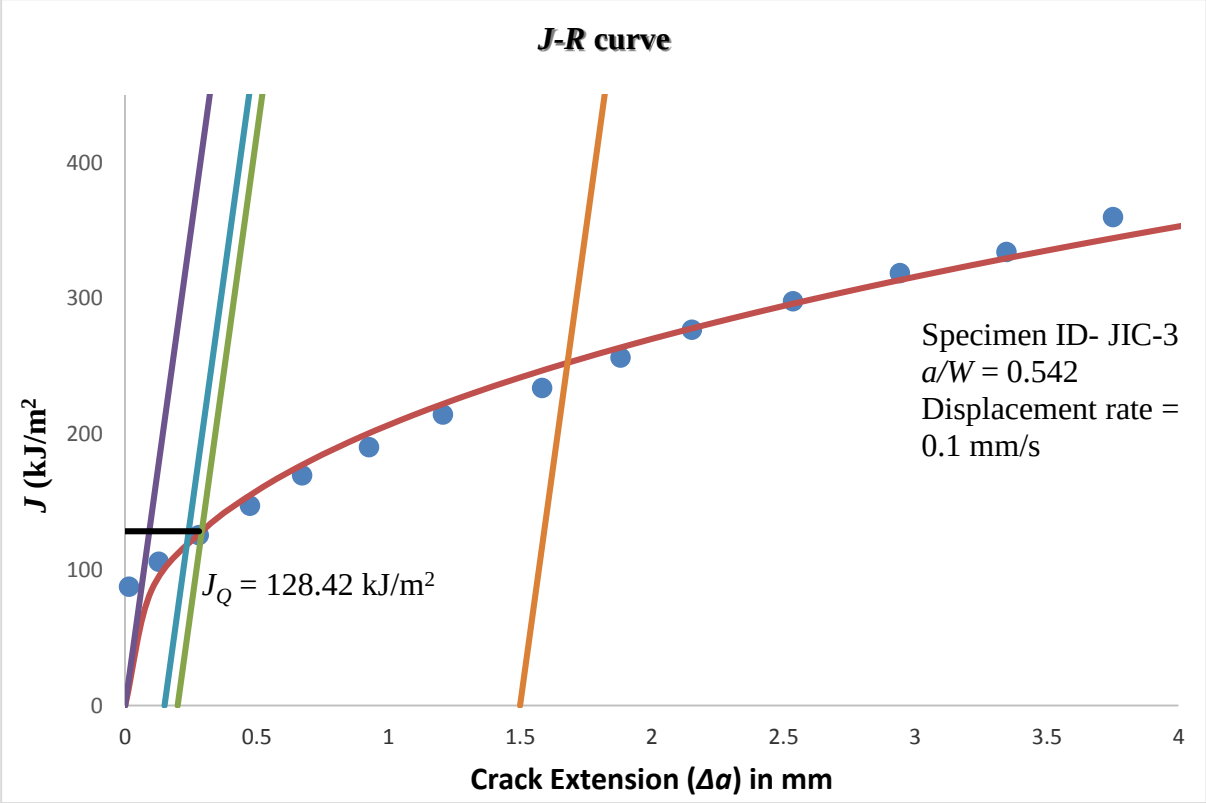

Figure 4.9 Typical *J-R* curve of specimen ID: JIC-3 at room temperature.

Table 4.3 Various J_{Ic} test parameter of investigate steel

Sample ID	a/W	bo (mm)	σ_Y (MPa)	Displace-ment rate (mm/s)	J_{limit} (kJ/m^2)	J_{max} (kJ/m^2)	Δa_{limit} (kJ/m^2)	Δa_{min} (mm)	Δa_{max} (mm)	J_Q (kJ/m^2)
JIC -1	0.45	27.94	700.536	0.05	2609.73	805.616	1.85	0.329	6.99	179.8
JIC -2	0.581	21.37	700.536	0.03	1996.061	837.14	1.82	0.336	5.34	228.2
JIC -3	0.542	23.37	700.536	0.1	2182.87	833.638	1.781	0.281	5.84	128.4

Table 4.4 Qualification criteria of J_Q as J_{Ic} and evaluation of K_{JIc}

Sample ID	J_Q (kJ/m^2)	bo (mm)	B (mm)	Thickness and initial ligament validity criteria (mm) $B, b_0 > \frac{10 J_Q}{\sigma_Y}$	Fulfilled The validity criteria?	Valid value of J_{Ic} As J_Q (kJ/m^2)	K_{JIc} (kJ/m^2) $= \sqrt{\left[\frac{E.J_{Ic}}{(1-v^2)}\right]}$
JIC -1	179.8	27.94	11.5	2.5666	Yes	179.8	205.845
JIC -2	228.2	21.37	11.95	3.2575	Yes	228.2	231.902
JIC -3	128.4	23.37	11.9	1.8329	Yes	128.4	173.952

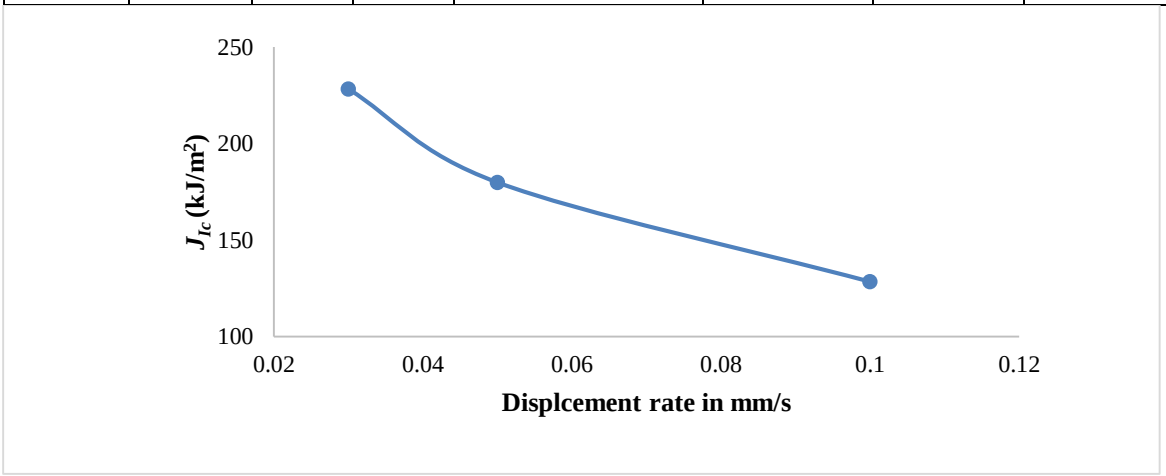

Figure 4.10. J_{Ic} vs. displacement rate curve

4.6.2 CTOD fracture toughness (δ_{Ic})

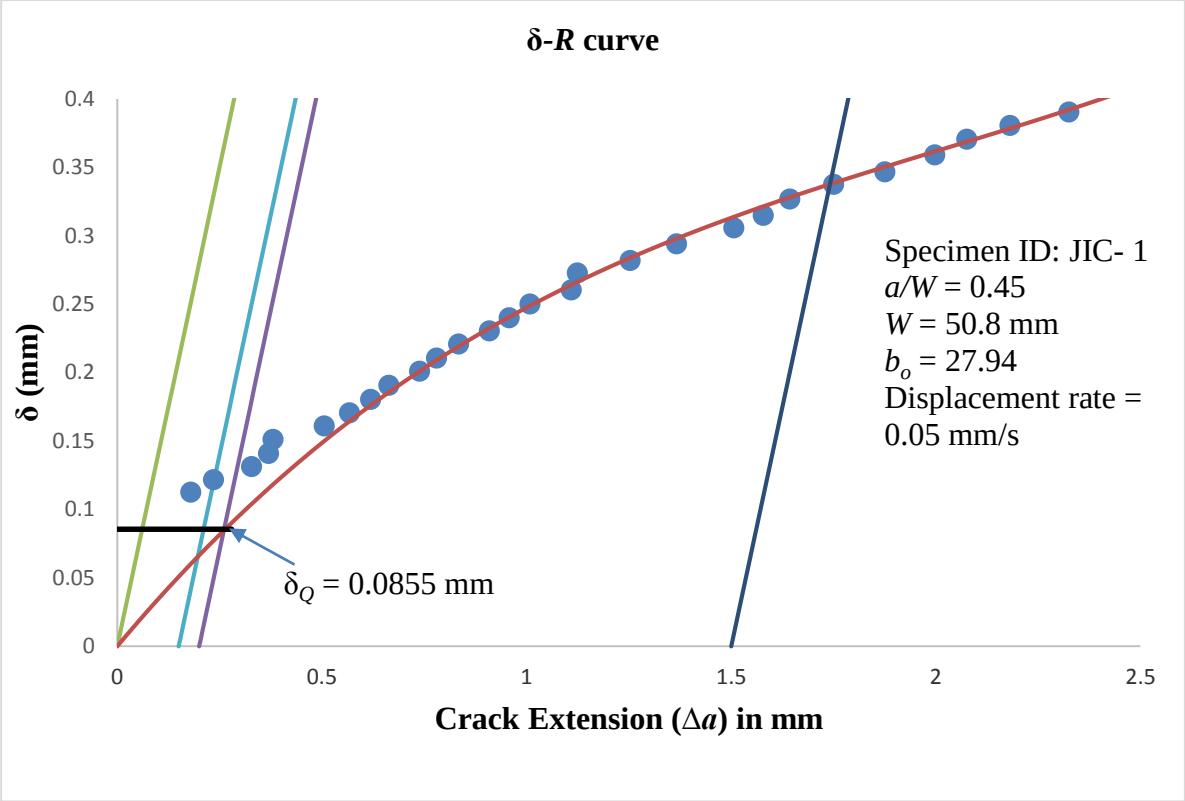

Figure 4.11 Typical δ-*R* curve of specimen ID: JIC-1 at room temperature.

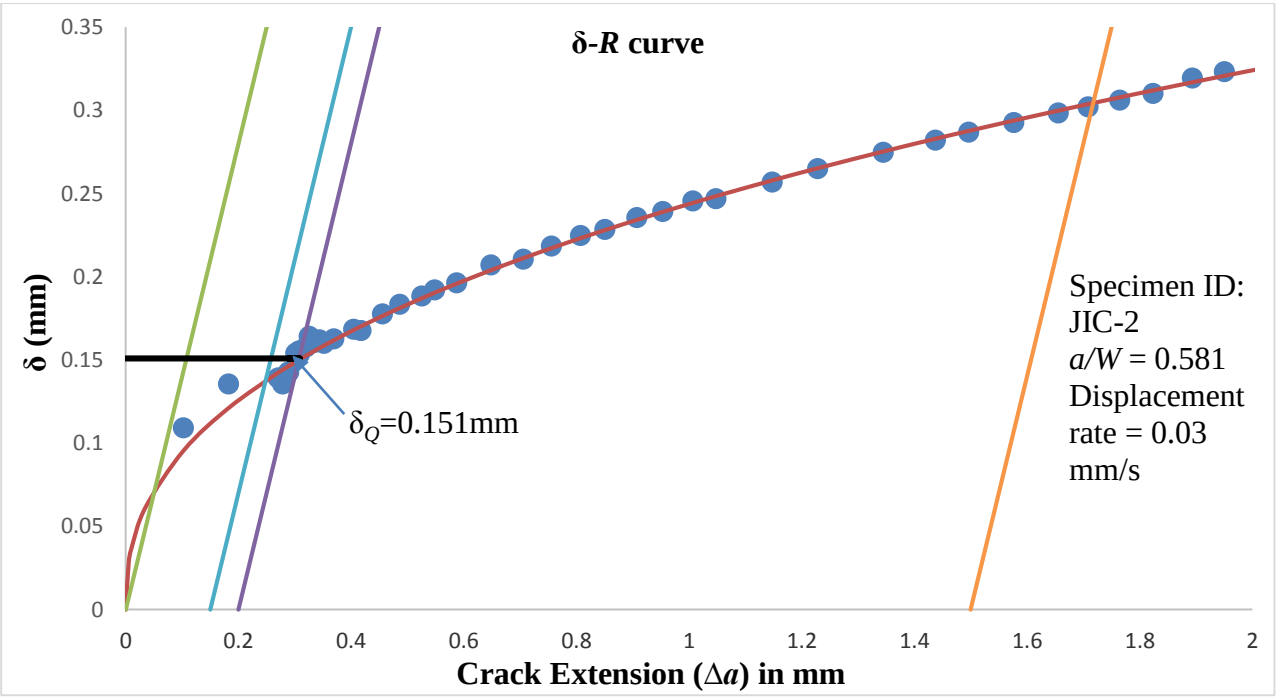

Figure. 4.12. Typical δ-*R* curve of specimen ID: JIC-2 at room temperature.

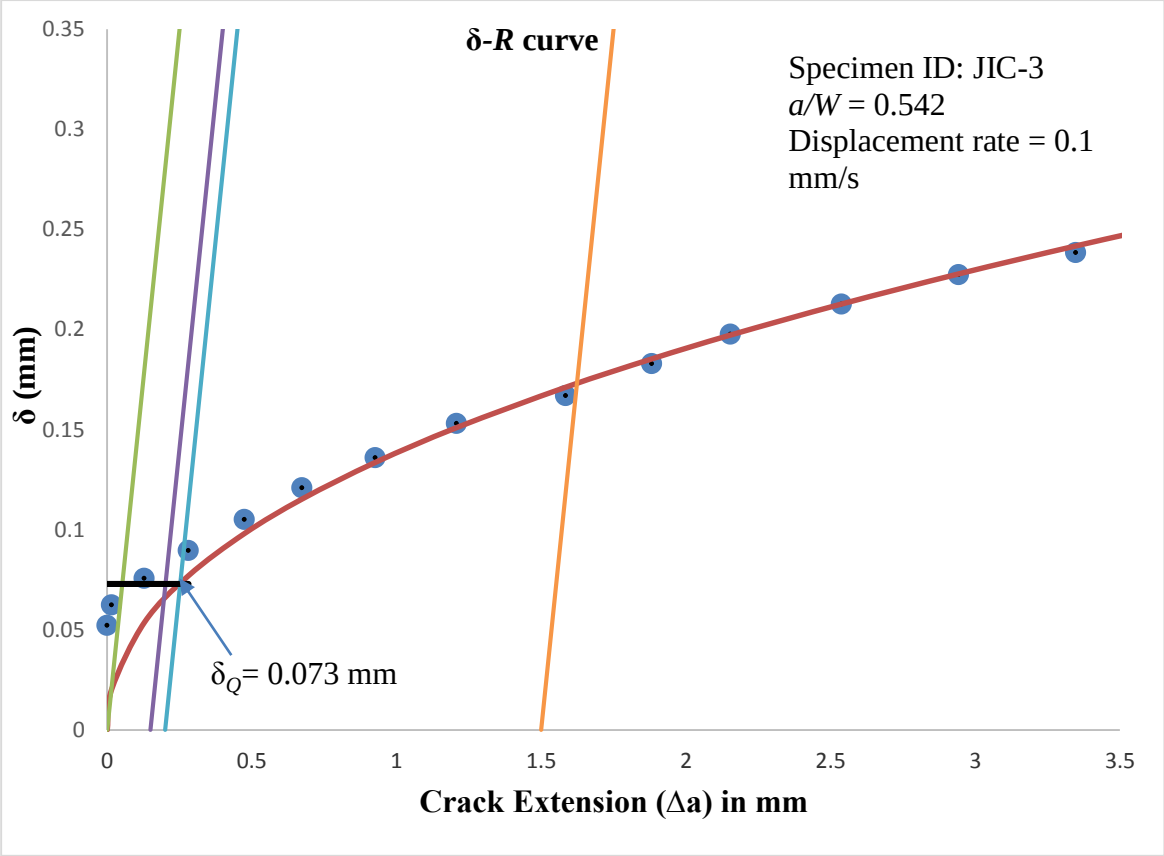

Figure 4.13. Typical δ-*R* curve of specimen ID: JIC-3 at room temperature.

Table 4.5 Various CTOD (δ) parameter of investigate steel

Sample ID	$\frac{a}{W}$	*bo* (mm)	Displacement rate (mm/s)	δ_{limit} (mm)	δ_{max} (mm)	Δa_{limit} (mm)	Δa_{min} (mm)	Δa_{max} (mm)	δ_Q (mm)
JIC -1	0.45	27.94	0.05	1.863	1.397	1.736	0.25	6.99	0.0855
JIC -2	0.581	21.37	0.03	1.425	1.0685	1.771	0.309	5.34	0.151
JIC -3	0.542	23.37	0.1	1.558	1.1685	1.629	0.281	5.84	0.073

Table 4.6 Qualification criteria of δ_Q as δ_{Ic}

Sample ID	δ_Q (kJ/m^2)	*bo* (mm)	initial ligament validity criteria $b_0 > 10m\delta_Q$ (mm)	Fulfilled The validity criteria?	Valid value of δ_{Ic} as δ_Q (mm)
JIC -1	0.0855	27.94	1.71	Yes	0.0855
JIC -2	0.151	21.37	3.02	Yes	0.151
JIC -3	0.073	23.37	1.46	Yes	0.073

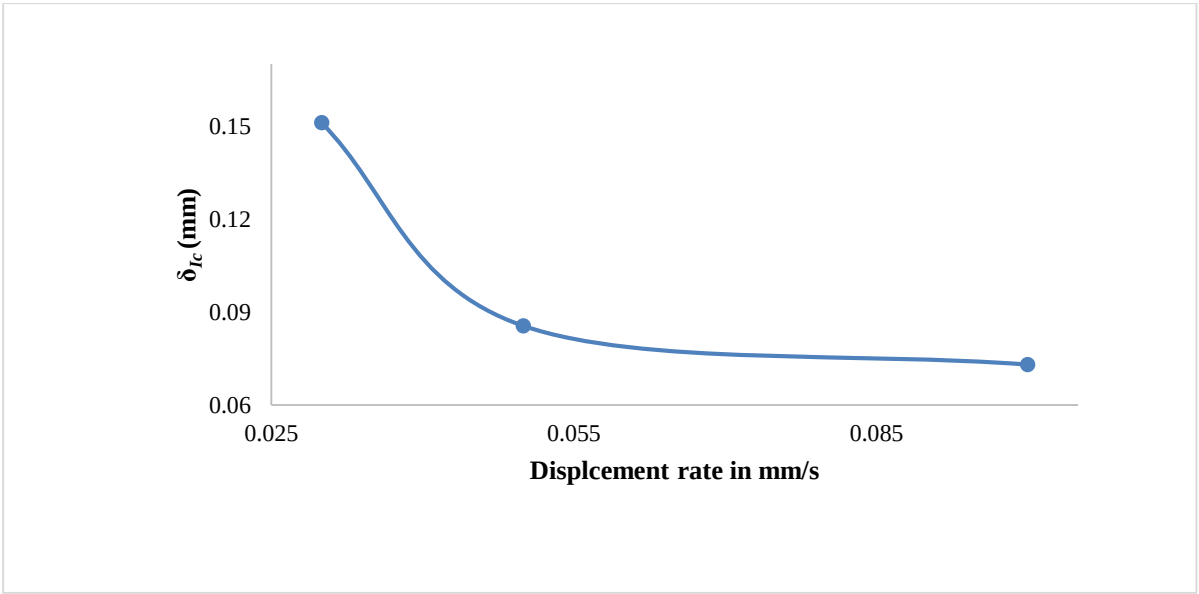

Figure 4.14 δ_{Ic} vs. displacement rate curve.

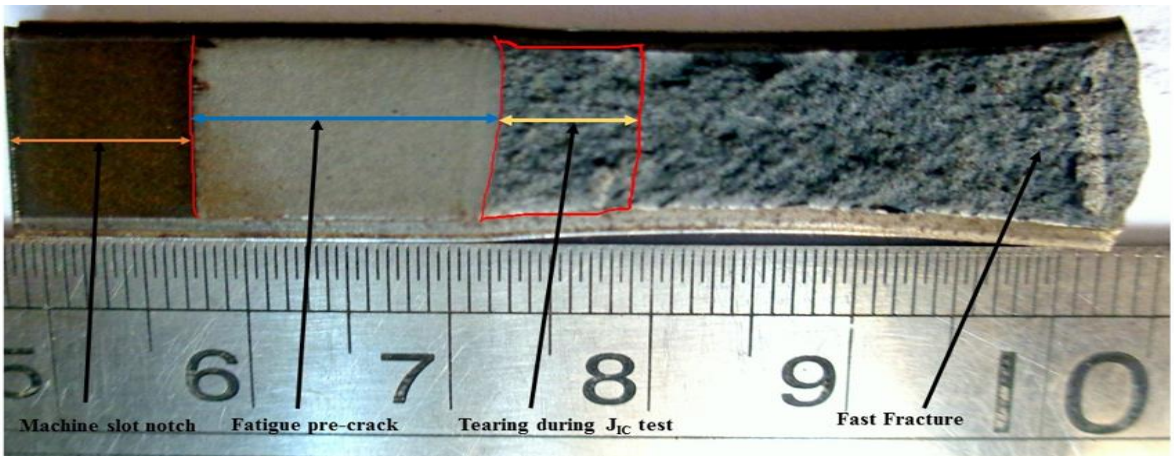

Figure 4.15 Typical fracture surface and various region of CT specimen (JIC-1) after fracture.

4.7 Fractogrphy of J_{Ic} test fracture surface

The fracture specimen were observed by FESEM, a typical micrograph of the initial region of the ductile crack extension is shown in figure 4.16 the fatigue pre-cracked region is found to be followed by an expanse of stretch zone (SZ), which in turn is followed by ridges dimples of ductile crack extension with all over microvoids are clearly visible.

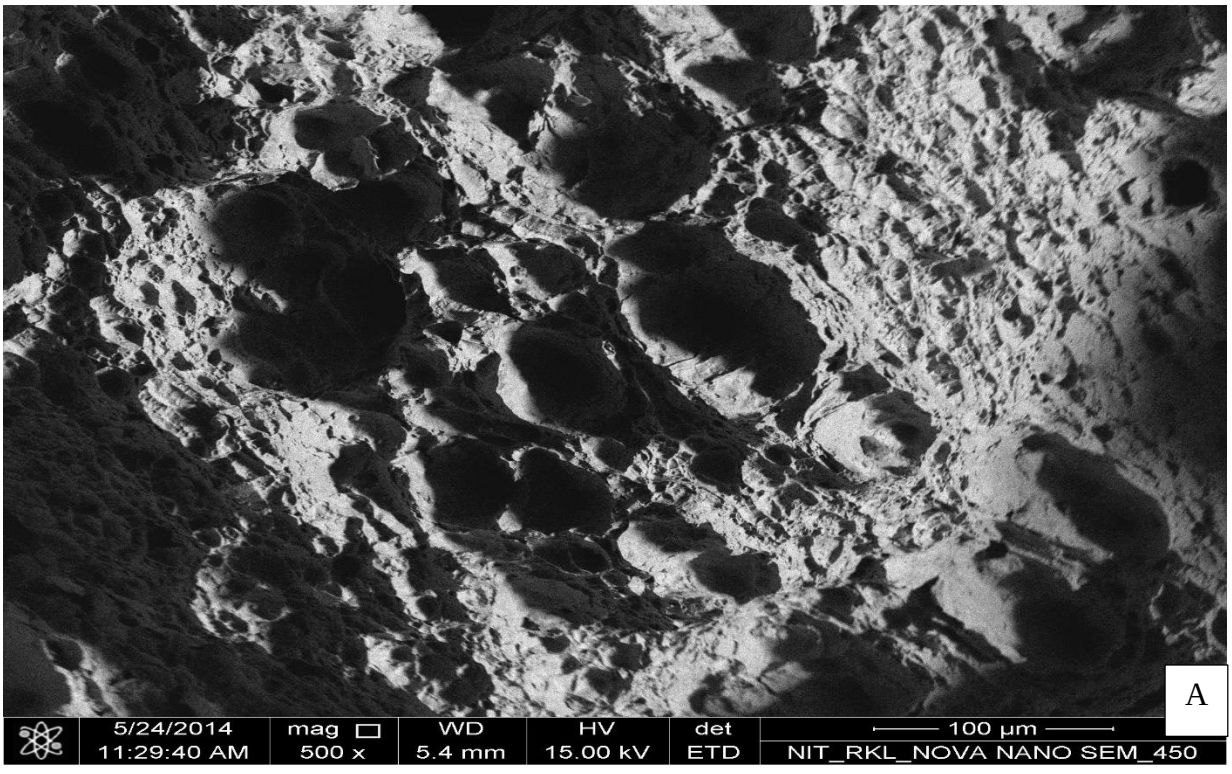

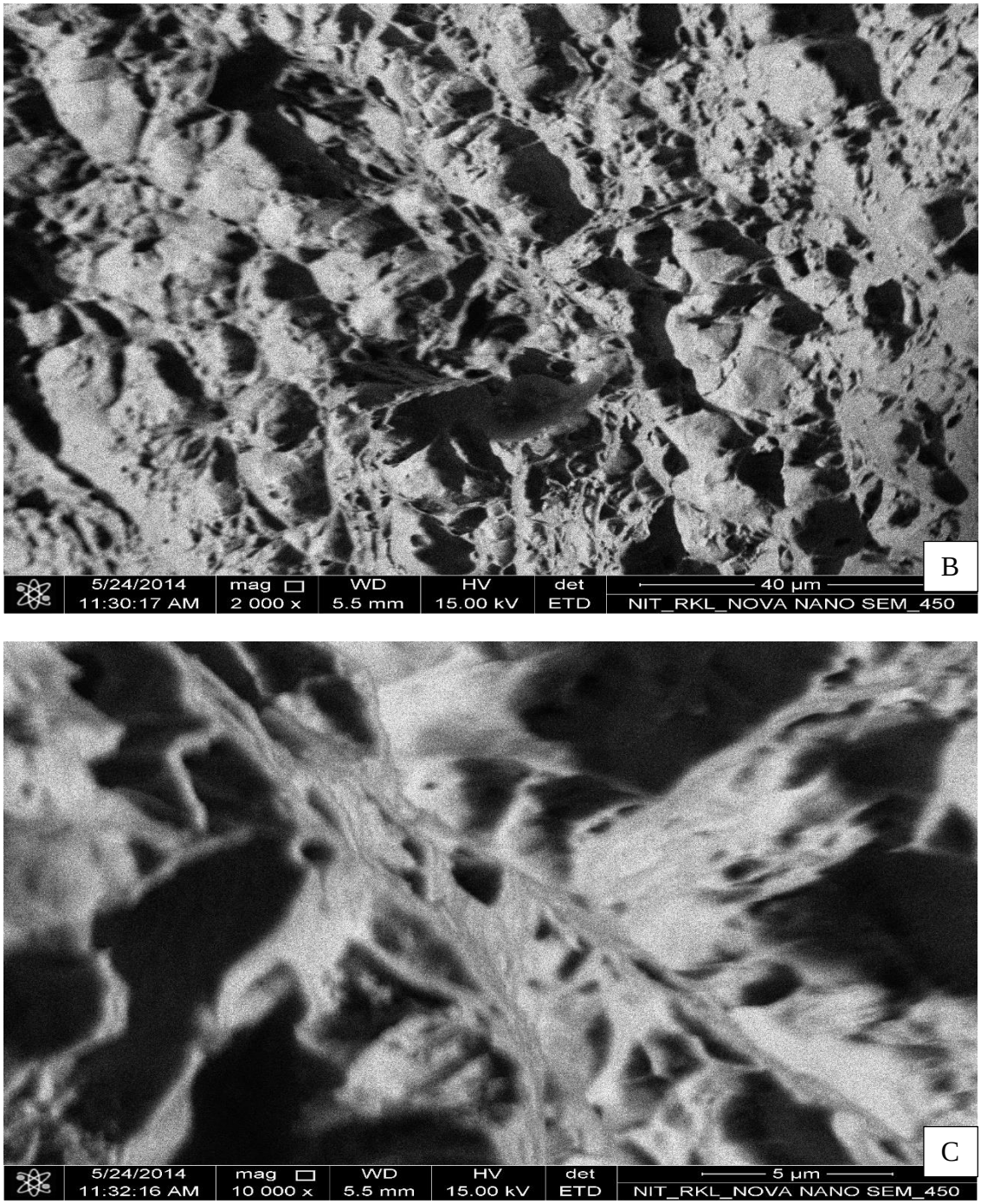

Figure 4.16. FESEM micrographs of JIC-1 specimen are presented above as:

A). FESEM micrograph shows dimpled fracture surfaces that are typical of microvoid coalescence.
B). High magnification of (A) showing the morphology of dimpled fracture surfaces and microvoid coalescence.
C). High magnification factograph of the HSLA steel ductile fracture surface.

4.8 Constant amplitude loading interposed with mode-I overload and band overload

The curve drawn between crack length and number of cycle, from the data obtained from the tests were normalization had done by the curve fitting procedure and the finally superimposed curves are plotted alongside with the base line data in figure 4.17 of the steel and figure 4.18 shows the log-log plot of crack growth rates vs. stress intensity factors range curves for different band overload. It is found that as the number of over load cycle increases amount of retardation decreases and for 7 overload cycle the retardation is maximum.

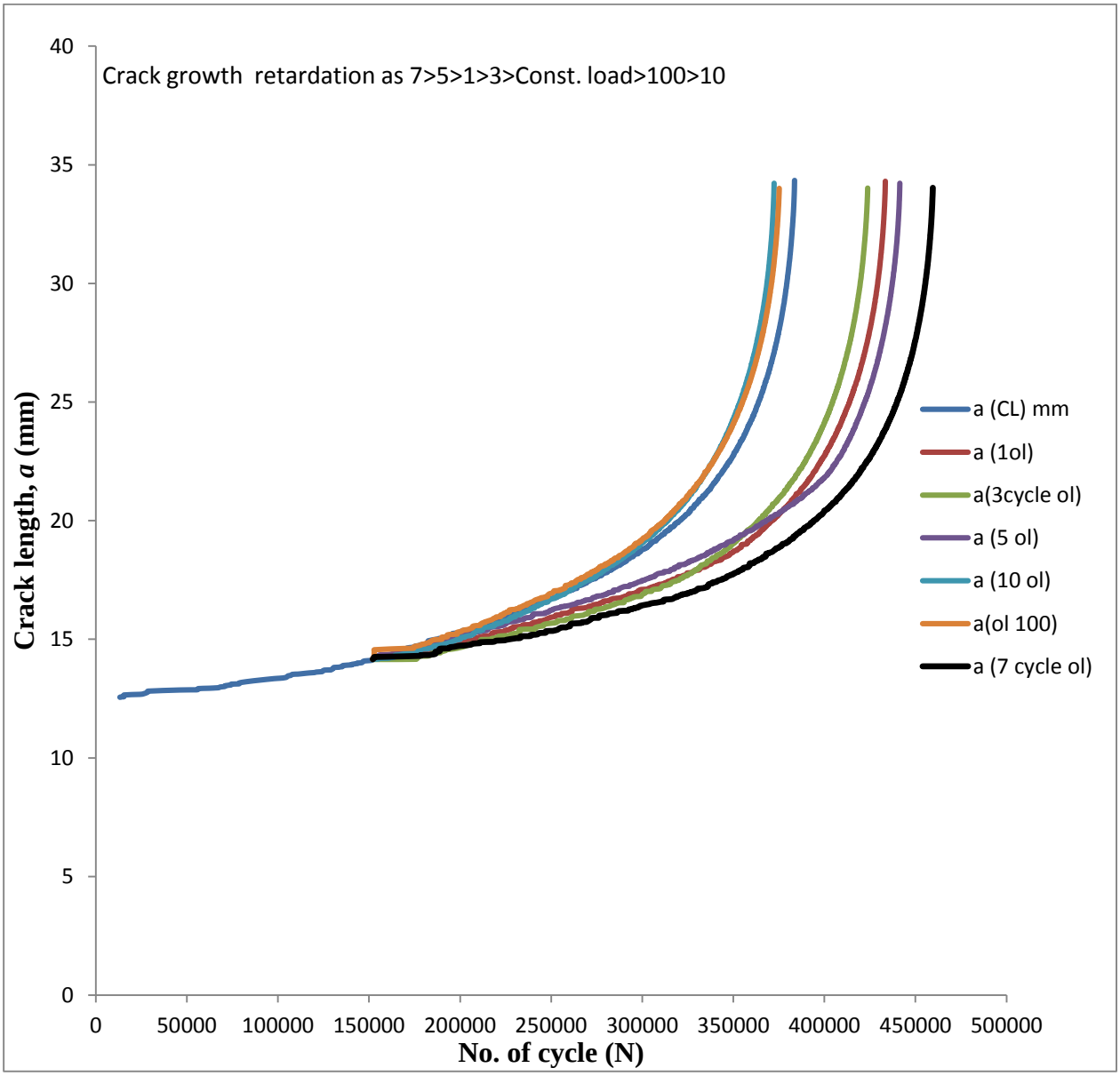

Figure 4.17 Superimposed crack length vs. number of cycle curve.

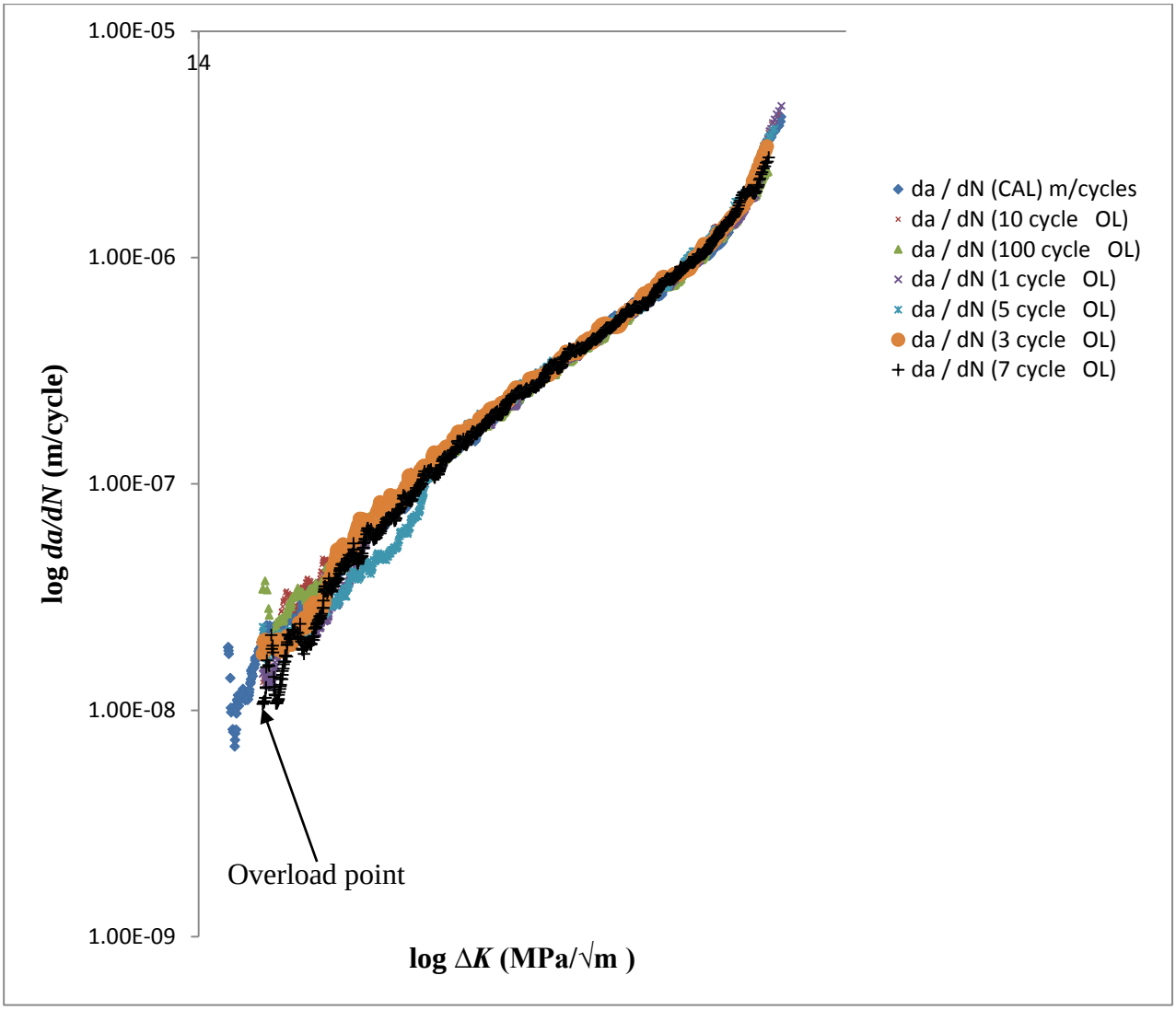

Figure 4.18– Superimposed log d*a*/d*N* versus log Δ*K* curve.

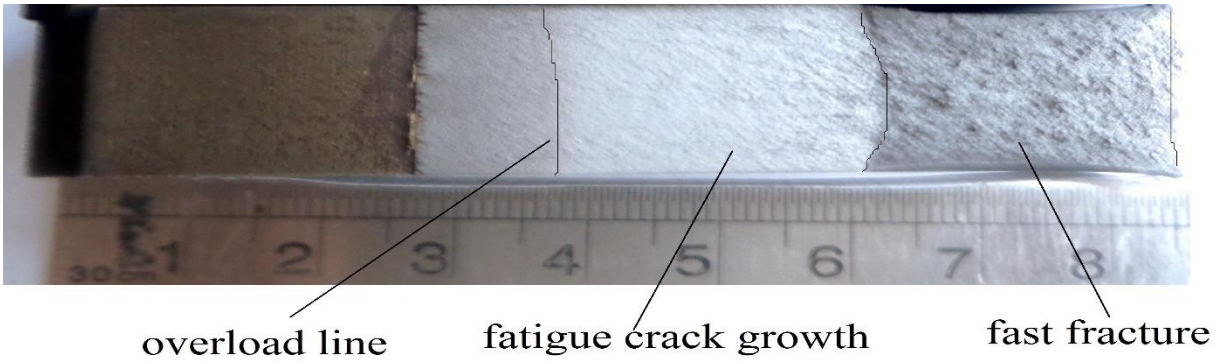

Figure 4.19 Various region of fracture surface of fatigue crack growth specimen imposed 7 cycle overload

4.9 Fractogrphy of fatigue fracture surface

Few representative specimens were examined under Field emission scanning electron microscope (FESEM). FESEM micrograph of constant amplitude loading test at R =0.3 are shown in Figure 4.20 and fractographs of an HSLA steel tested at R_{ol} = 1.25 are presented in Figure 4.21. Although the surface indicates the presence of striations.

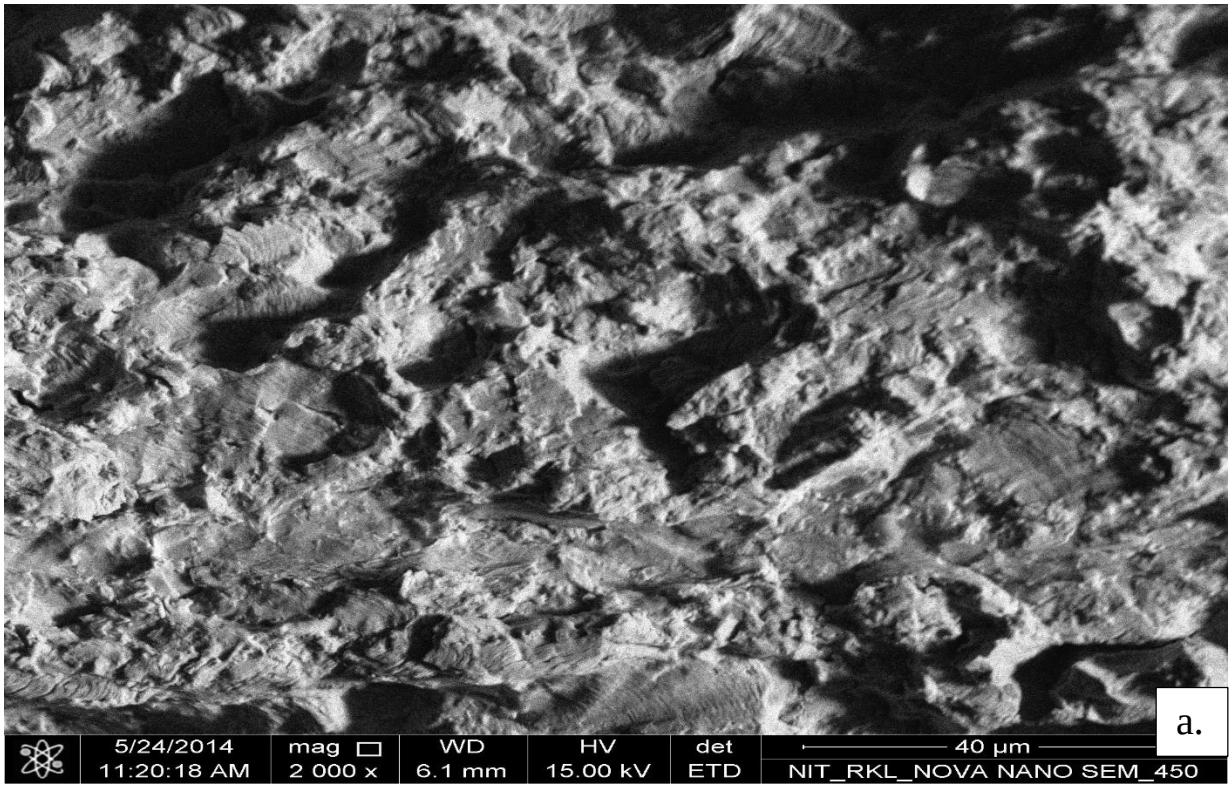

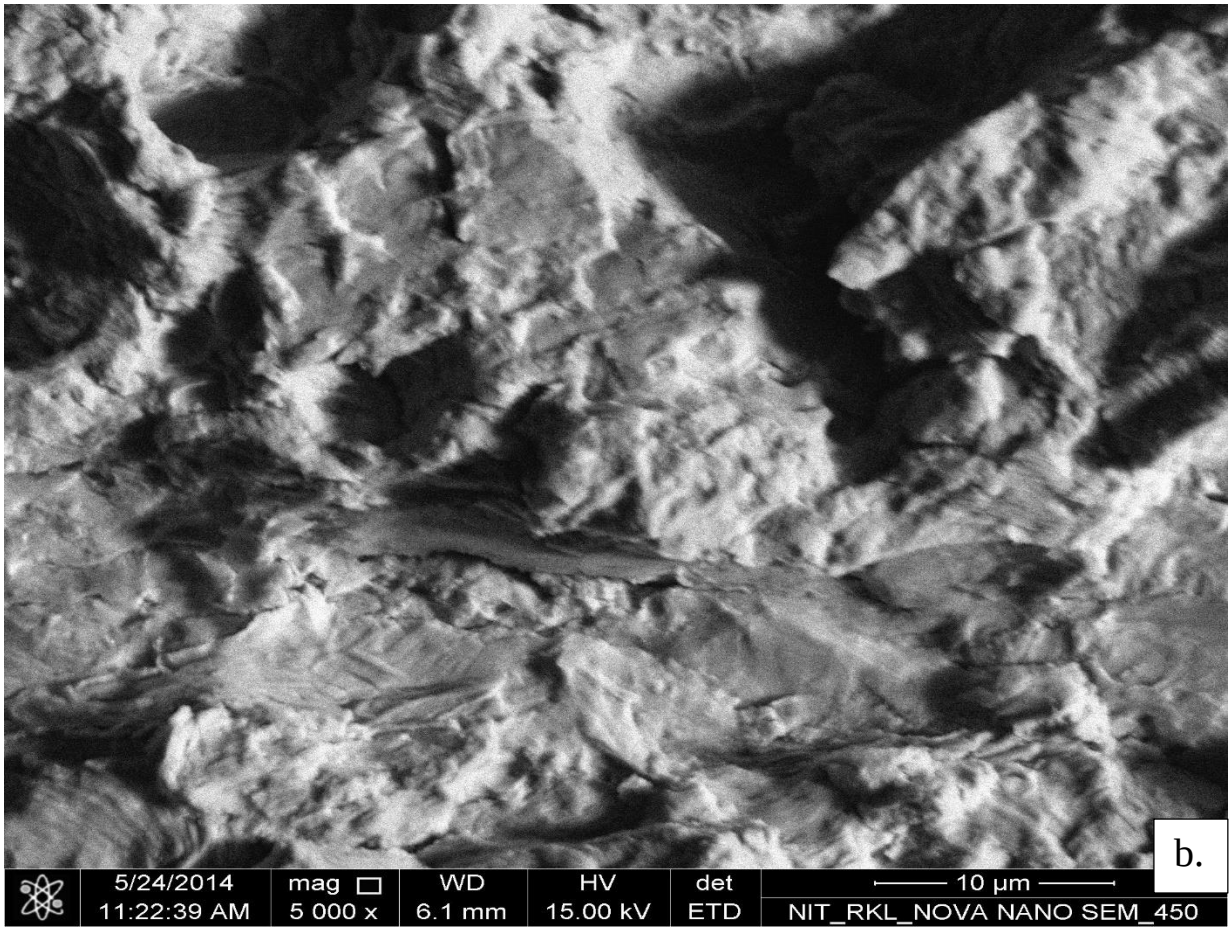

Figure 4.20 FESEM micrographs of the constant amplitude load fatigue tested fracture surface of an HSLA steel at stress ratio (R) = 0.3.
a.) A microscopic cracks and fine microscopic cracks with stable crack growth.
b.) In high magnification showing shallow striations in the region of stable crack growth.

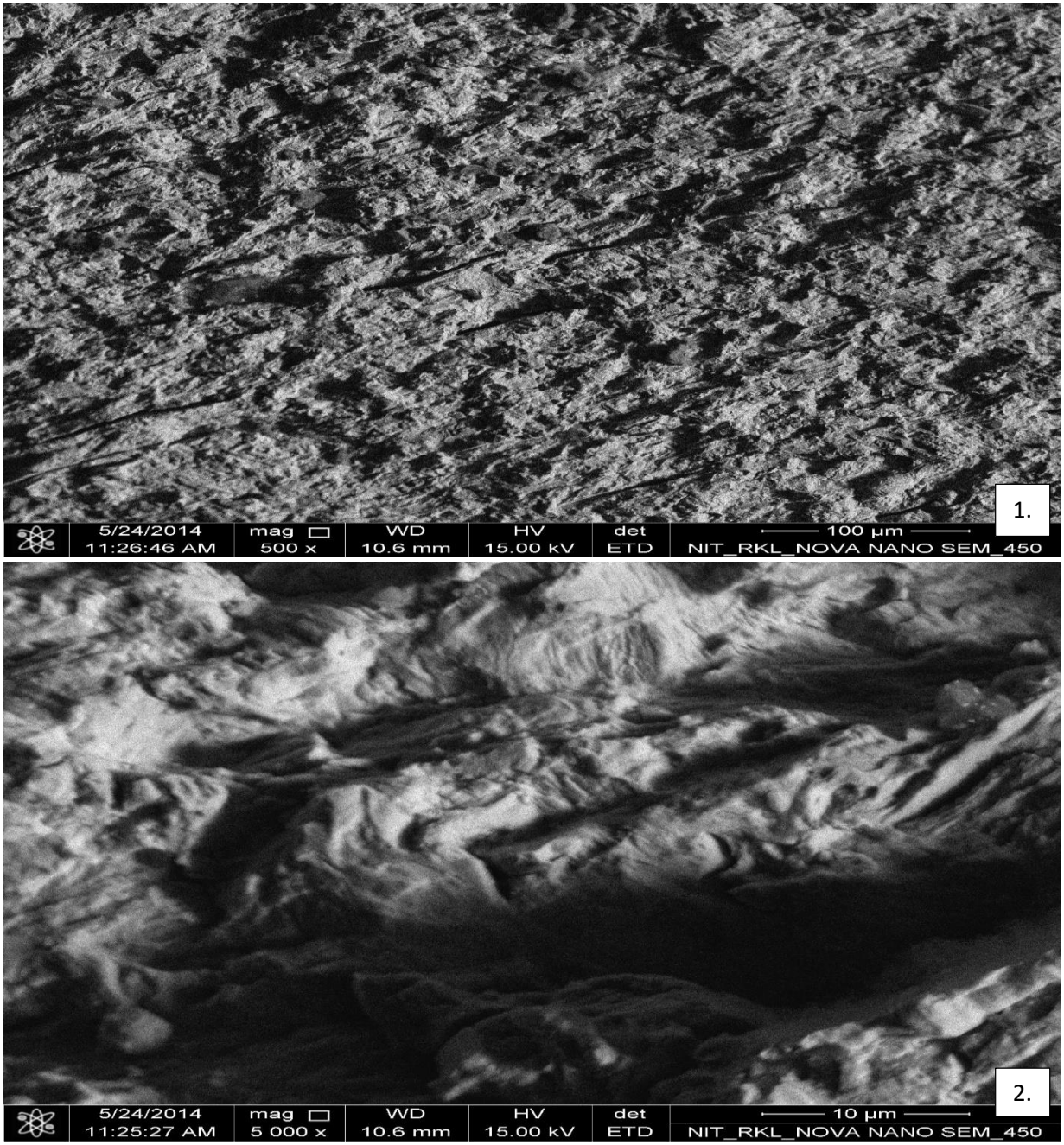

Figure 4.21 FESEM micrographs of the constant amplitude load imposed with 7 cycle tensile overload fatigue tested fracture surface of steel at overload ratio (R_{ol}) = 1.25.

1.) Overall morphology of fracture surface.

2.) In high magnification showing shallow striations absence of microvoides hinds insignificant gross plastic deformation during overloading.

Chapter 5

CONCLUSIONS AND FUTURE WORK

5.1 Conclusions

In the present work, the elastic plastic fracture toughness test and fatigue crack growth study was conducted on 1- CT specimen with reduced thickness of an HSLA steel.
The J_{Ic} tests were performed under three different displacement rate and finally the effect of displacement rate on fracture toughness are studied.
In fatigue crack growth study three different loading conditions were applied: constant amplitude loading with fixed stress ratios, constant loading interspersed with single spike overload, and constant amplitude loading interspersed with multiple (band) spike overload. Effect of overload and band overload on fatigue growth life are determined.
The conclusions drawn from the present work are summarized as follows:

1. The J_Q fracture toughness values of 1-CT specimens with reduced thickness prepared from the as received steel fulfills the validity criteria according to ASTM E-1820-13 standard. This J_Q value can be used as fracture toughness value of this steel.
2. The experimental results of fracture toughness test show that the elastic plastic fracture toughness parameters J_{Ic} and δ_{Ic} decrease with increasing displacement rate.
3. The application of overload and band overload reduces the crack growth rate. However, the extent of retardation is little (applied R_{ol} =1.25).
4. Maximum retardation was observed on application of 7 overload cycles.
5. This enhanced retardation effect is explained on the basis of large plastic strain field zone formed at the crack tip. The subsequent overload application may have resulted some crack extension and reduced the effectiveness of plastic strain field region.

5.2 Suggested future work

(1) Fracture toughness test were carried out at three displacement rates only. However need to be conducted over a wide range of displacement rates.
(2) The fracture toughness studies were done at room temperature. It is suggested to conduct the test at low temperatures and elevated temperatures. Similar work may also be done on the welded joints of an HSLA steel.
(3) Attempts may be made to use the model to predict fatigue life under overload and band overload conditions.
(4) Fatigue crack growth studies may also be conducted applying realistic spectrum variable amplitude conditions.
(5) Strain field distribution may be obtained using soft computing and CAE software under various conditions

Chapter 6

REFERENCE

REFERENCES

[1] Brog TK, Jones JW, Was GS. Fatigue Crack Growth Retardation of INCONEL600. Engineering Fracture Mechanics. 20 (1984); No. 2, pp. 313-320.

[2] Sander M, Richard HA. Finite element analysis of fatigue crack growth with interspersed mode-I and mixed mode overloads. International Journal of Fatigue. 27 (2005); pp. 905-913.

[3] Sander M, Richard HA. Experimental and numerical investigations on the influence of the loading direction on the fatigue crack growth. International Journal of Fatigue. 28 (2006); pp. 583-591.

[4] Anderson T L., Fracture Mechanics: Fundamentals and Applications. Boston CRC Press, 1995.

[5] Mohanty JR, Verma BB, Ray PK. Prediction of fatigue crack growth and residual life using an exponential model: Part II (mode-I overload induced retardation) International Journal of Fatigue. March 31 (2009); pages 425-432.

[6] Narasaiah N, Tarafder S, Sivaprasad S. Effect of crack depth on fracture toughness of 20MnMoNi55 pressure vessel steel. Materials Science and Engineering. A257 (2010); 2408-2411.

[7]. Rice JR. A Path Independent *J*-Integral and the Approximate Analysis of Strain Concentration by Notches and Cracks. Journal of Applied Mechanics June 35 (1968); pp. 379.

[8] Hertzberg, Richard W. Deformation and Fracture Mechanics of Engineering Materials (4 ed.) 1995; Wiley ISBN0-470-01214-9.

[9] Griffith AA. The Phenomena of Rupture and flow in solids. Philosophical Transitions of the Royal Society of London. A221 (1921); pp. 163-169.

[10] Irwin GR. Analysis of stresses and strains near the end of a crack traversing a plate. Journal of Applied Mechanics. 24 (1957); pp. 361-364.

[11] Wells AA. Application of fracture mechanics at and beyond general yielding. Br Weld J. 10 (1963); pp. 563–570.

[12] Xian-Kui Zhu, James A. Joyce. Review of fracture toughness (*G, K, J, CTOD, CTOA*) testing and standardization. Engineering Fracture Mechanics 85 (2012); pp. 1–46.

[13] Clarke GA, Andrews WR, Begley JA, Donald JK, Embley GT, Landes JD, et al. A procedure for the determination of ductile fracture toughness values using J integral techniques. J Test Evaluates. 7(1979); 49–56.

[14]. Standard Test Method for Plane-Strain Fracture Toughness of Metallic Material. Annual Book of ASTM Standards, E1820-2013

[15] Barsom Jhon M, Rolfe Stanley T. Fracture and fatigue control in structures: Applications of Fracture Mechanics, ASTM stock Number: MNL41, 1999.
[16] Kodama S., Misawa H, Hasegawa H, Nakayama H. The effect of strain rate on the J-Integral. Engineering Fracture Mechanics (1978).
[17] Bannantine Julie A, Comer Jess J, Handrock James L. Fundamentals of Metal Fatigue Analysis, Prentice Hall, Englewood Cliffs, New Jersy 1990.
[18] Ellyin F, Li HP. *"*Fatigue crack growth in large specimens with various stress ratios*"*. Journal of Pressure Vessel Technology. 106 (1984); pp. 255–260.
[19] Gdoutos EE. Fracture Mechanics- An Introduction, Springer,2005.
[20] Broek, D, Elementary Engineering Fracture mechanics, Martinus Nijhoff Publishers, The Hague,1982.
[21] Schijve J. Significance of Fatigue Cracks in Micro-Range and Macro-Range, Fatigue Crack Propagation, ASTM STP 415, American Society for Testing and Materials, Philadelphia, 1967.
[22] McMillan JC, Pelloux RMN. "Fatigue Crack Propagation Under Program and Random Loads," ASTM STP 415, American Society for Testing and Materials, Philadelphia, 1967.
[23] Von Euw E F J, Hertzberg RW, Roberts R, Delay Effects in Fatigue Crack Propagation. ASTM STP 513, American Society for Testing and Materials, Philadelphia, 1973.
[24] Jones RE. Fatigue Crack Growth Retardation After Single-Cycle Peak Overload in Ti6A1-4V Titanium Alloy. Engineering Fracture Mechanics 5 (1973).
[25] Wei RP, Shih TT. Delay in Fatigue Crack Growth. International Journal of Fracture, 10 (March 1974).
[26] Hardrath, HF McEvily AT. Engineering Aspects of Fatigue-Crack Propagation. Proceedings of the Crack Propagation Symposium, Cranfield, England, 1 (October 1961).
[27] Schije J, Jacobs FA, Tromp, PJ, Crack Propagation in Clad 2024-T3A1 Under Flight Simulation Loading. Effect of Truncating High Gust Loads. NNLR TR-69050-U, National Lucht-En Ruimtevaart-Laboratorium (National Aerospace Laboratory NLR-The Netherlands), June 1969.
[28] Hudson C M, and Hardrath H F. Effects of Changing Stress Amplitude on the Rate of Fatigue-Crack Propagation of Two Aluminum Alloys, NASA Technical Note D-960, NASA, Cleveland, September 1961.
[29] Von Euw EFJ. Effect of Single Peak Overloading on Fatigue Crack Propagation. Master's dissertation, Lehigh University, Bethlehem, PA, 1968.
[30] Wheeler OE. Spectrum Loading and Crack Growth. General Dynamics Report FZM-5602, Fort Worth, June 30, 1970.
[31] Willenborg J, Engle RM, and Wood HA, A Crack Growth Retardation Model Using an Effective Stress Concept. Technical Memorandum 71-1-FBR, Air Force Flight Dynamics Laboratory, January 1971.
[32] Elber W. The Significance of Crack Closure, Damage Tolerance in Aircraft Structures. ASTM STP 486, American Society for Testing and Materials, Philadelphia, (1971), pp. 230-242.

[33] Wei RP, Shih TT. Delay in Fatigue Crack Growth. International Journal of Fracture. 10, No. 1 (March 1974).
[34] Von Euw E F J, Hertzberg RW, Roberts R, Delay Effects in Fatigue Crack Propagation. ASTM STP 513, American Society for Testing and Materials, Philadelphia, 1973.
[35] Gardner FH, Stephens RI. Subcritical Crack Growth Under Single and Multiple Periodic Overloads in Cold-Rolled Steel. ASTM STP 559, American Society for Testing and Materials, Philadelphia, 1974.
[36] Trebules Jr VW, Roberts R, Hertzberg RW, Effect of Multiple Overloads on Fatigue Crack Propagation in 2024-T3 Aluminum Alloy. ASTM STP 536, American Society for Testing and Materials, Philadelphia, 1973.
[37] Standard Test Methods for Tension Testing of Metallic Materials. Annual Book of ASTM Standards, E8/E8M-13a, 2013.
[38] Indian Standard METHOD FOR CHARPY IMPACT TEST (U-NOTCH) FOR METAL UDC 620.178.746.22:669, IS: 1499 – 1977, Reaffirmed 2003.
[39] Standard Test Method for Measurement of Fatigue Crack Growth Rates, Annual Book of ASTM Standards, E647, 2013.